Damage of SRC Building Structures by 1995 Hyogo Earthquake

Junichi SAKAI
Research Assistant
Kyushu University
Fukuoka, Japan

Junichi Saka, born 1962,
received master degree of Eng.
from Kyushu Univ. in 1989.
His research interests are
analyses of beam-columns,
joints, and frames in steel and
composite structures.

Koichi MINAMI
Professor
Fukuyama University
Fukuyama, Japan

Koichi Minami, born 1939,
received Dr. of Eng. from
Kyoto Univ. in 1985. His
research interests are analysis
of beam-columns, joints, and
frames in RC and composite
structures.

Chiaki MATSUI
Professor
Kyushu University
Fukuoka, Japan

Chiaki Matsui, born 1937,
received Dr. of Eng. from
Kyoto Univ. in 1971. His
research interests are analyses
of beam-columns, joints, and
frames in steel and composite
structures.

Summary

A large number of Steel Reinforced Concrete (SRC) building structures were damaged seriously
owing to 1995 Hyogoken-Nanbu Earthquake in Japan. The authors have investigated the damage
of buildings and collected the data of 1,307 SRC buildings in and around Kobe city. Thirty-one
SRC buildings collapsed by the story failure. All of them were constructed before 1972 and open-
web type steels were used in SRC members. In this paper examples of damage of SRC buildings
and members, and statistical analysis of damage are described.

1. Introduction

Steel Reinforced Concrete (SRC) building structure did not sustain severe structural damage owing
to Kanto earthquake (1923) and has been developed as reliable earthquake resistant structure in
Japan. Miyagiken-Oki Earthquake (1978) was the first strong earthquake that modern SRC
structures had experienced. About three hundred high-rise buildings were shaken in Sendai city.
Then cracks were observed in many nonstructural reinforced concrete exterior walls of high-rise
apartment houses, however structural skeletons such as beams and columns were not damaged
even though accelerations of 100 percent of gravity acceleration g were recorded in the upper
stories [1].

Hyogoken-Nanbu Earthquake occurred on January 17, 1995 with a magnitude 7.2 on the Richter
scale by Japan Meteorological Agency. Its epicenter was located close to a densely populated
area. The earthquake caused severe damage to building structures and over 5,500 people were
killed due to fire and collapsed buildings resulting from the severe shaking.

Hyogoken-Nanbu Earthquake was the first time that a large number of SRC buildings were
subjected to severe structural damage. The distinctive feature of collapsed buildings was the
story failure at an upper floor level, and most part of the collapsed buildings with mid-height

failure were constructed of SRC structures or mixed structures with SRC members in lower stories and reinforced concrete members in upper stories, in Sannomiya area, the downtown of Kobe city, where many office buildings and commercial buildings stand.

2. Damage of SRC Buildings

SRC members can be divided into two types. One of them is called open web type SRC, that was composed of angle steel as principal steel components and steel sections were fabricated with angles arranged to form lattices or ladders by rivet or bolt (see Fig. 2). This type of SRC had been used for most of SRC buildings constructed before 1975. The other is called full web type SRC, that is composed of H shaped steel as principal steel components (see Fig. 2). After 1968, it had made clear by some tests that earthquake resistant performance of SRC members using open web type steel was worse than one using full web type steel from the view point of shear behavior [2].

A new seismic code has been introduced in 1981, the ultimate strength of the structure and member ductilities under lateral load are considered, and the required lateral strength is given as a function of the deformation capacity assigned to various building types and members. With revising the code, the full web type SRC has been used for most of the SRC buildings constructed since then.

Figure 2 shows the relation of SRC type and construction year of buildings, and the construction years are divided into six periods according to the revising of the standards for structural calculation of SRC structures published by Architectural Institute of Japan [3] (AIJ standard). The term IV (1975-1980) show the period that buildings were constructed with either open web type or full web type.
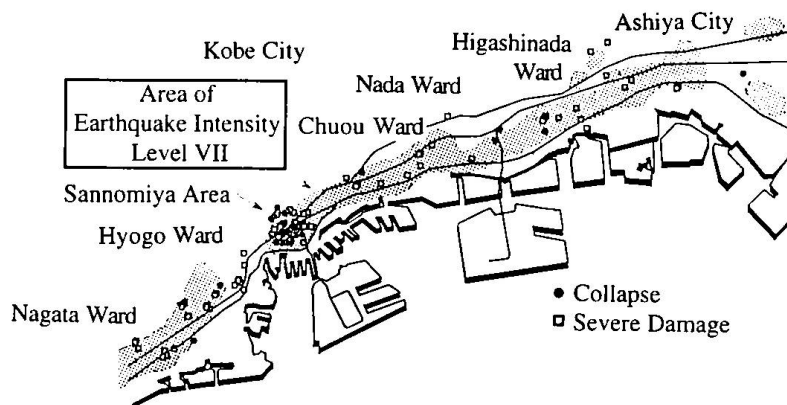

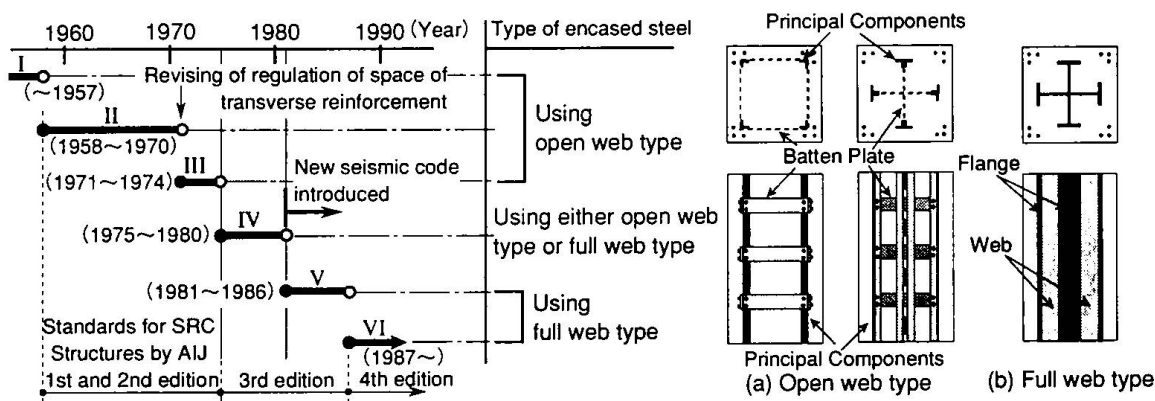*Fig. 1 Distribution of SRC buildings subjected collapse or severe damage.*

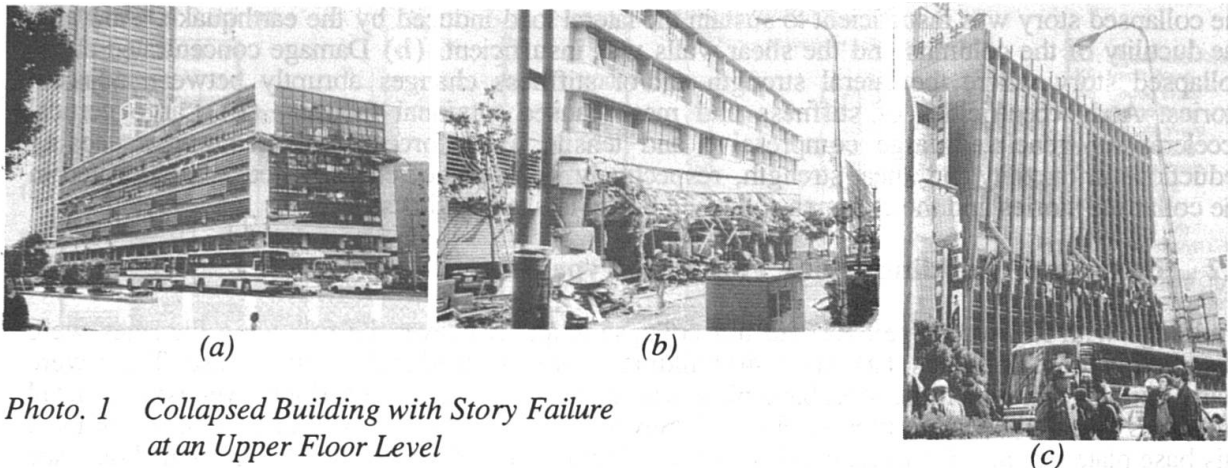*Fig. 2 Decision of Classification of Years of Completion of Buildings*

(a)   (b)

Photo. 1   Collapsed Building with Story Failure
at an Upper Floor Level

(c)

Photo. 2   Collapsed Column in Shear
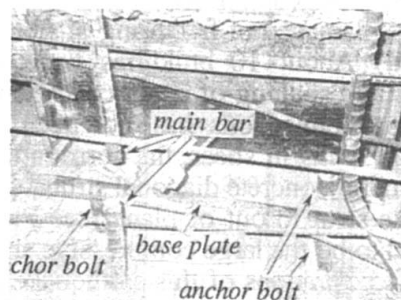
Photo. 3   Fracturing of
Anchor Bolt at Column Base
(after chipping concrete)
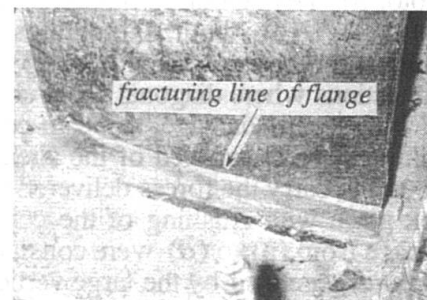
Photo. 4   Fracturing of
Column Steel Flange Plate
(after chipping concrete)

Photo. 6 Damage of
Beam-Column Connection
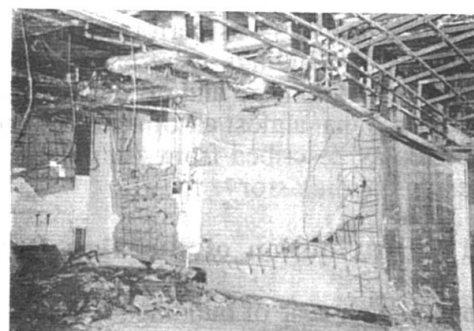
Photo. 7 Damage of RC Shear Wall

Photo. 5   Fracturing of Splice Plate at Column Joint (after chipping concrete)

2.1   Collapsed Buildings with Open Web Type SRC

Thirty-one of SRC buildings collapsed by the story failure. All of them were constructed before 1972 and composed of the open web type SRC. Twenty-seven buildings collapsed by the story failure at an upper floor level (see Photo. 1) and four buildings collapsed   at the first story.   At the failure story, SRC columns collapsed brittly in shear (see Photo. 2) and concrete in RC shear walls crushed to out of plane. Collapse by the story failure at an upper floor level was characterized of the damage caused by this earthquake.   Several factors potentially responsible for these failures can be considered as follows: (a) The design earthquake force distribution over the height used in the old design codes is different from the one used now, and the proportion of design story shear force is smaller at the mid-stories in the old codes. Then the ultimate strength of

the collapsed story was insufficient to sustain the lateral load induced by the earthquake. And also the ductility of the columns and the shear walls was insufficient. (b) Damage concentrated at the collapsed story where the lateral strength and/or stiffness changes abruptly between adjacent stories. And eccentricities of stiffness and mass caused torsional failure. (c) Large vertical accelerations generated large compressive and tensile axial forces in the columns, causing reductions in ductility and shear strength, respectively. (d) Joint of encased steel was located in the collapsed stories and the columns collapsed brittly in shear at this story.

2.2 Damage of Buildings with Full Web Type SRC

Buildings with full web type SRC did not collapse at all. However the following damages were observed in these buildings: (a) About 40 buildings were damaged at the column base. There were many buildings in which the steel base plate was anchored at the ground floor level using a detail known as "non-embedment type steel base". Severe damage was observed in buildings that used this base plate detail.   Concrete crushed at the column base and anchor bolts were pulled out (see Photo. 3) . (b) About 10 buildings were damaged of fracturing of   encased steel flange plate (see Photo. 4).   (c) About 10 buildings were damaged of fracturing of steel splice plate at the joints of columns or beams (see Photo. 5). (d) About 10 buildings were damaged at beam-column connections where diagonal shear cracks and spalling of cover concrete were observed (see Photo. 6), but severe damage at beam-column connections has not been reported.   (e) About 40 buildings were damaged of the shear RC walls in shear; the surrounding SRC frame was strong enough to carry the forces delivered from the concrete diagonal struts, so sliding failure of the wall took place with crushing of the concrete strut to out of plane (see Photo. 7).   Reasons for the damage from (a) to (d) were considered to be the large compressive and tensile axial forces in the columns generated by the large vertical accelerations of this earthquake and the existence of multi-story shear walls.   A large number of columns or beams with flexural cracks, shear cracks, and shear bond cracks were observed, but severe damage has not been reported.

3   Statistical Analysis of Damage of SRC Buildings

Statistical analysis was performed by data of damage of 1,307 buildings in and around Kobe city. Damages of buildings were classified into six groups, that were collapse, severe, intermediate, minor, slight damage and no damage. Damage of 260 buildings has not been clear, but it can be considered that almost all of them sustained under minor damages.   Statistical analysis of damage degree was described from the point of construction year, regional group of buildings, building use and building story.

3.1   Distribution of Building Damage Classified by Construction Year

Construction year of buildings was divided as shown in Fig. 2. Distribution of building damages classified by construction years is shown in Fig. 3. The ratio of the number of the buildings collapsed or sustained severe damage to the total of buildings constructed before 1970 was up to 30 percent (40/134), and the ratio of buildings constructed before 1974 was 26 percent (70/266). Almost all of them were composed of open web type SRC. On the other hand, with full web type SRC constructed after 1981, only 3 percent of buildings sustained severe damage (18/618), and no such a building collapsed.

3.2   Distribution of Building Damage Classified by Regional Group

3.2.1   Distribution of Building Damage Classified by Location
Distribution of building damage classified by locations is shown in Fig. 4. Locations are nine ward of Kobe city, Ashiya city, Nishinomiya city, Itami city, Takarazuka city, Amagasaki city and Akashi city. The number of SRC buildings constructed in chuou ward of Kobe city was 462, and the ratio of this number to all buildings was 35 percent.   In this ward, 26 buildings collapsed, 40 buildings were subjected to severe damage, and the ratio of the number of buildings sustained those damage to total buildings was 15 percent.
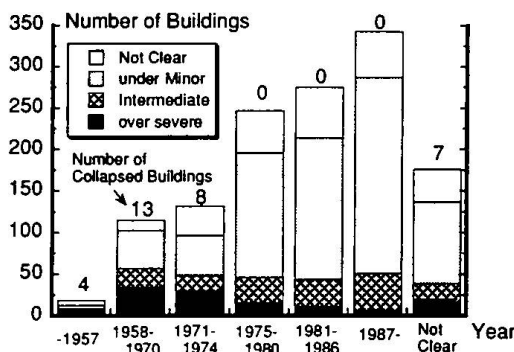
Fig. 3 Damage Classified by
Construction Years
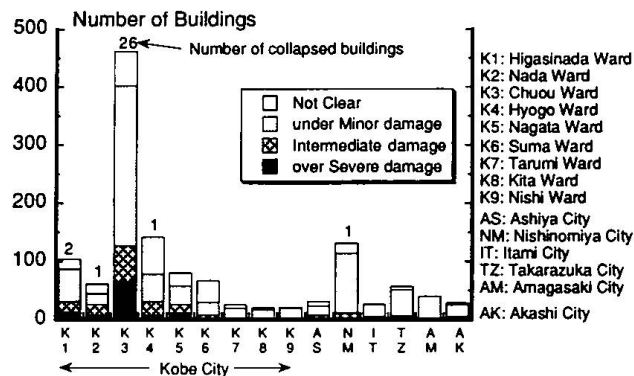
Fig.4 Damage Classified by Locations
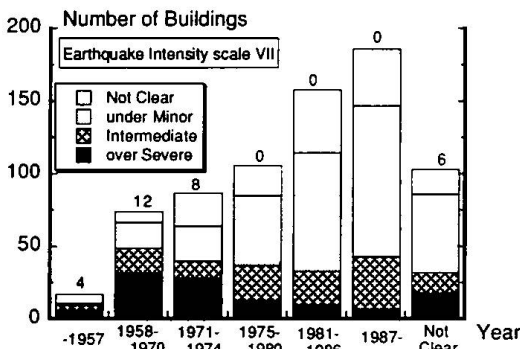
Fig. 5 Damage in Area of Earthquake
Intensity Level VII

Fig. 6 Damage Classified by Building Use

(a) Collapse or Severe Damage

(b) Intermediate Damage
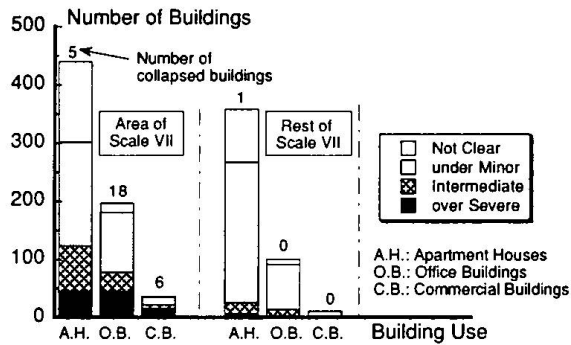
(c) under Minor Damage
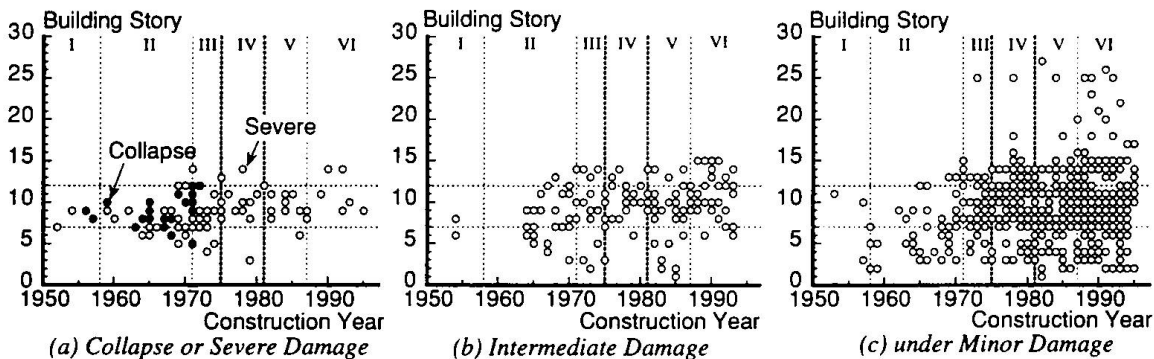
Fig. 7 Damage Classified by Story and Construction Year

3.2.2 Distribution of Building Damage Classified by Area of Earthquake Intensity Scale

An earthquake intensity scale is defined eight grade scales by Japanese Meteorological Agency. The intensity scale VII is the most intense grade, where the maximum acceleration of ground motion   is over 400 gal. The area of earthquake intensity scale VII (area VII) spread widely in and around Kobe city. The area VII was defined on the map by Geographical Survey Institute of Japan, and M. Murakami presumed the address of the area from this map [4]. The ratio of the number of buildings constructed in the area VII to the total of buildings was 56 percent (731 buildings). Figure 5 shows the distribution of the building damage classified by construction years   in the area VII. The buildings constructed before 1974 in the area VII tended to be subjected severer damage, and about half of the buildings constructed from 1958 to 1970 collapsed or sustained severe damage(32/74).   On the other hand, only 5 percent   of buildings constructed after 1981 sustained severe damage (17/344).

3.3   Distribution of Building Damage Classified by Building Use

Buildings were divided by building use as apartment houses, office buildings, commercial buildings and the others (see Fig. 6). The ratio of the number of apartment houses, office buildings and commercial buildings to the total of buildings were 61 percent (802 buildings), 23 percent (298) and 4 percent (49), respectively. The number of collapsed buildings were 5, 19 and 7 for apartment houses, office buildings and commercial buildings, respectively. The ratio of the number of commercial buildings collapsed or sustained severe damage to the total of buildings constructed in the area VII was up to 43 percent (16/37). The ratio for office buildings and for apartment houses   was 23 percent (45/197) and 16 percent (45/441), respectively.

3.4   Distribution of Building Damage Classified by Building Story

Figure 7 shows the distribution of damage classified by building story and construction years. From these figures, it was clear that almost all of the buildings collapsed or sustained severe damage had over seven to twelve stories, and the buildings under six stories tended to be able to avoid severe damage, regardless of construction years of buildings. The buildings over fifteen stories did not sustain severer damage.

4   Conclusions

It has been made clear from performing analysis of damage of SRC buildings that;

1) Thirty one SRC building structures were collapsed with the story failure.   All of them were constructed before 1972 and composed of open web type SRC. The distinctive feature of damage of SRC buildings was the story failure at an upper floor level, and 27 buildings collapsed in this type.   No building structure with full web type SRC collapsed at all.

2) Some buildings with the full web type SRC sustained severe damage. The feature of the damage was as follows; crushing of concrete at the column base and/or pulling out of anchor bolts, fracturing of steel flange plates, fracturing of steel splice plates at the joints, crack of concrete at the beam-column connections, and shear failure of RC walls surrounding the SRC frames.

3) Buildings using the open web type SRC constructed before 1974 tended to sustain to severer damage. In the earthquake intensity scale VII, half of the buildings constructed from 1958 to 1970 collapsed or sustained severe damage. On the other hand   only 5 percent of   buildings constructed after 1981 sustained severe damage in this area.   The ratio of the number of commercial buildings collapsed or sustained severe damage to the total of buildings constructed in this area was up to 43 percent.   Almost all of the buildings collapsed   or   sustained severe damage had over seven to twelve stories, and the buildings under six stories tended to be able to avoid severe damage.   The buildings over fifteen stories did not sustain severer damage.

References
[1] AIJ, Report on the Damage Due to 1978 Miyagiken-Oki Earthquake, Chapter 7, Damage of SRC Buildings, Feb. 1980, pp. 595-629 (in Japanese).
[2] M. Wakabayashi and K. Minami, Experimental Studies on Hysteretic Characteristics of Steel Reinforced Concrete Columns and Frames, International Symposium on Earthquake Structural Engineering, St. Lousis, Missouri, USA, 1976.
[3] AIJ, Standards for Structural Calculation of Steel Reinforced Concrete Structures, June 1987.
[4] AIJ, Report on the Damage of Concrete Structures Due to 1995 Hyogoken-Nanbu Earthquake, Kinki branch of AIJ, July, 1996 (in Japanese).
[5] K. Minami, Analysis of SRC Building Structures Damaged during the 1995 Hyogoken-Nanbu Earthquake, Concrete Journal Vol. 34, No. 11, Nov. 1996, pp. 34 - 36 (in Japanese).

Detailing Requirements for Concrete-Filled Steel Tubes Connections

Stephen P. SCHNEIDER
Professor
University of Illinois
Urbana, IL, USA

After receiving his M.S.C.E., Stephen P. Schneider worked several years at Skilling Ward Magnusson Barkshire, Inc a structural engineering firm in Seattle, WA. Among other notable buildings, this firm designed Two Union Square which is well known for its use of concrete-filled steel tubes and high performance concrete. In 1991, Stephen P. Schneider received his Ph.D. in Civil Engineering at which time he joined the faculty at the University of Illinois.
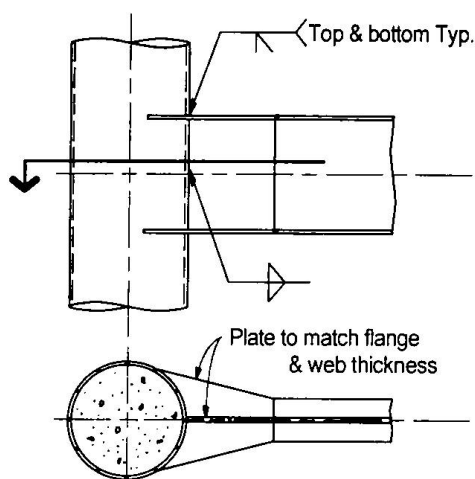
Summary

This paper summarizes experimental research on connections to concrete-filled steel tubes. Results suggested that transferring the girder force exclusively to the face of the tube wall led to fracture of the tube wall, flange and weld. External diaphragms alleviated extreme deformation demand on the tube, and enabled the connection to develop the flexural strength. Connections with components that penetrated the tube wall initiated a plastic hinge in the connected girder. However, inelastic cyclic behavior depended on the type of elements embedded.
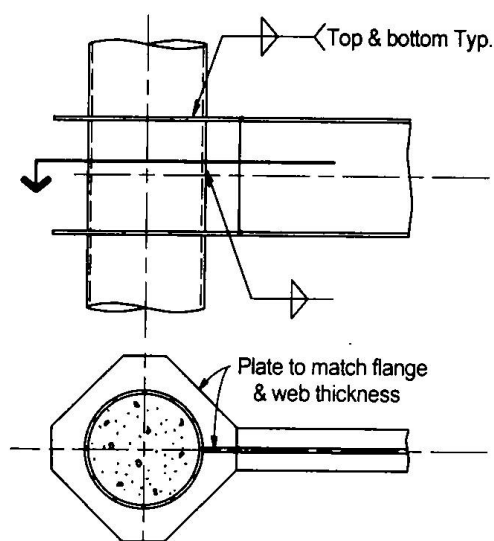
1. Introduction

Concrete-filled tube [CFT] columns provide many advantages over the more conventional reinforced concrete or structural steel columns. Some of these advantages include: the steel tube provides formwork for the concrete core, the concrete prolongs local buckling of the steel tube wall, the tube prohibits excessive concrete spalling, and the composite column adds significant stiffness compared to traditional steel frame construction. While many advantages exist, the use of CFTs in building construction has been limited. This lack of use is due, in part, to limited construction experience and to the complexity of connection detailing. This paper summarizes part of an experimental program to study a variety of details to connect a steel girder to a circular CFT column.

Test data exists on a variety of connection details. Details that connect the girder to the steel tube only include: welding the girder directly to the tube skin (Valbert, 1968), using web angles or shear tabs to connect the girder to the tube (Shakir, 1992; Bridge, 1992), providing external or internal diaphragms (Kato et. al., 1992; Morino et.al., 1992), and variations on the above details (Ansourian, 1976). Conclusions from these studies suggest that connections loading the steel tube exclusively can cause excessive deformation demand on the tube wall and connection components. Connections that attempted to improve this behavior include: through bolting girder end plates (Prion et. al., 1992; Kanatani et. al., 1987), and continuing structural steel shapes through the column (Azizinamini et. al., 1992). Comparison of test data suggests that embedding connection components into the concrete core alleviates high shear demand on the tube wall, which may improve the seismic performance of the connection. The object of this research was to investigate the inelastic flexural behavior of a wide range of connection details.

Six connections tested in this research program are shown in Fig. 1. The primary interest of this research program was to investigate connections that develop the flexural strength of the

Type I: Simple Welded Connection

Top & bottom Typ.

Plate to match flange & web thickness

Type II: Diaphragm Plate Connection

Top & bottom Typ.

Plate to match flange & web thickness
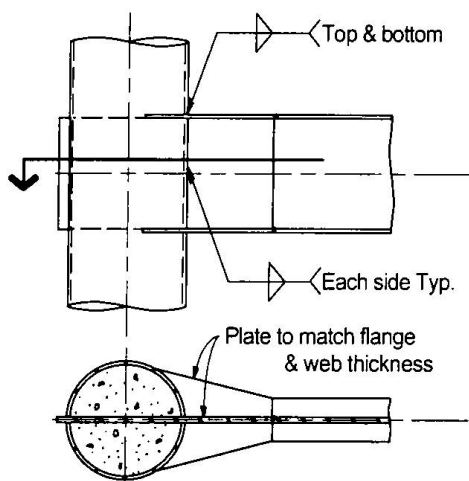
Type III: Continuous Web Connection

Top & bottom

Each side Typ.

Plate to match flange & web thickness
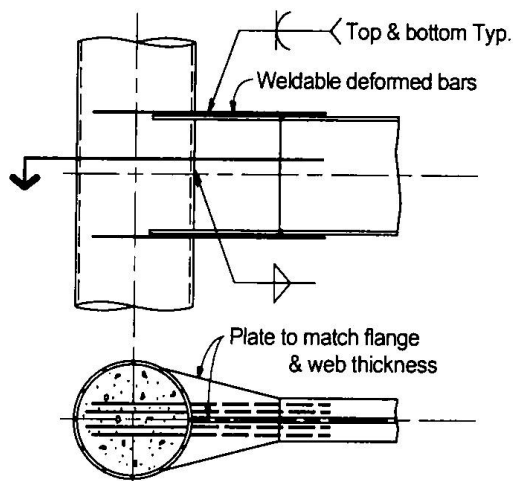
Type IV: Embedded Deformed Bar Connection

Top & bottom Typ.

Weldable deformed bars

Plate to match flange & web thickness
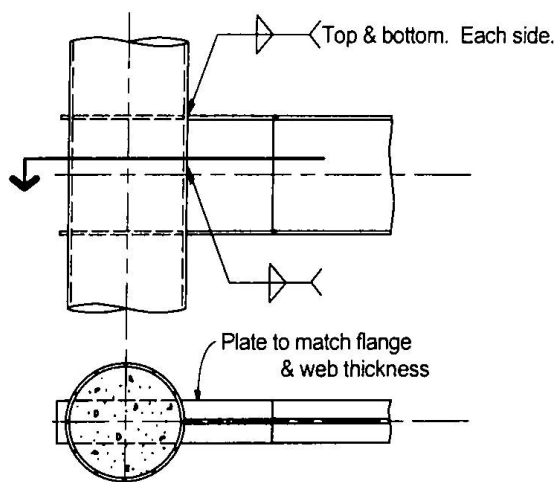
Type V: Continuous Flange Connection

Top & bottom. Each side.

Plate to match flange & web thickness
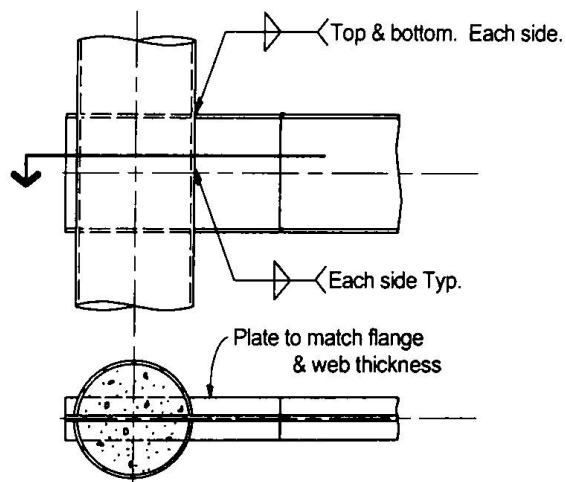
Type VI: Continuous Girder Connection

Top & bottom. Each side.

Each side Typ.

Plate to match flange & web thickness

Figure 1. Connection Details

connected girder. Since connection behavior was the primary interest, and not joint or panel zone behavior, the girder connected to only one side of the CFT column was sufficient. Because of the difficulty in connection detailing, only circular tubes were considered. Each test specimen consisted of a *356 mm* diameter pipe with a *6.4 mm* wall thickness, and a *W14x38* for the girder. The yield strength for the pipe and the girder was *320 MPa*, with an approximate concrete strength of *35 MPa*. Cyclic deformation were imposed on all girders according to the *ATC-24* (1992) guidelines for the cyclic testing of components.

2. Experimental Study

The inelastic, cyclic moment-rotation [M- θ] behavior for each connection is shown in Fig. 2. The moment was normalized with respect to the plastic bending strength of the girder.

For the simple *Type I* connection, the girder was welded directly to the skin of the steel tube. Consequently, the steel tube was subject to high local distortions adjacent to the connected region. Fracture initiated in the connection stub flange, at a rotation of 1.5%. This fracture propagated into the tube wall at approximately 3.2% rotation. This tearing propagated from the tips of the flange toward the web. Only one flange fractured, the tube wall separated from the concrete core as the other flange was subjected to tension. This resulted in an unsymmetric M-θ behavior, and a pinching of the hysteretic curves. Degradation in flexural strength began once the flange fractured, and continued upon subsequent deformation cycles. This fracture precipitated high shear demand on the web plate, which led to fracture of the weld between the web and the pipe wall. Consequently, the girder lost all shear capacity shortly after flange failure.

The external diaphragms of connection *Type II* were intended to alleviate the severe distortion on the steel tube skin. These diaphragms improved the cyclic behavior of the simple connection significantly. One diaphragm fractured at approximately 0.5% rotation, while the other diaphragm fractured at almost 1.0% rotation. Upon subsequent cycles, the fracture propagated in each diaphragm, eventually tearing the tube wall at a rotation of 3.5%. Deterioration of the M-θ behavior occurred at the onset of diaphragm fracture. At large cyclic displacements, the diaphragm buckled, and the tube wall fractured along the depth of the girder.

The intent of the continuous web *Type III* detail was to improve the shear behavior of the simple Type I connection. However, significant web tearing was still observed once the flanges failed. Similar to the simple connection, the flange fracture exacerbated the high strain demands on the extreme fibers of the web. Due to embrittlement of the web in the heat affected zone, tearing initiated close to the fillet weld that attached the web to the pipe wall. Fracture initiated at approximately 1.25% rotation, precipitating a 20% decrease in peak flexural strength by the end of these imposed deformation cycles. Eventually, this fracture propagated from each flange toward the center of the web. A significant portion of the web was fractured by approximately 2.5% rotation, resulting in poor hysteretic performance of the connection for larger imposed rotations.

Connection *Type IV* was identical to connection *Type I*, except four *20 mm* ϕ (F_y = *420 MPa*) weldable deformed bars were embedded in the concrete core through holes drilled in the steel tube wall. Each deformed bar was then welded to the girder flange. Embedment lengths were sufficient to develop the deformed bar under tested conditions. The M-θ behavior of this detail was a significant improvement compared to connection *Type I*. Initial wall tearing was observed at 3.5% rotation. However, this tearing was located only in the tube wall between the openings for the deformed bars. This minor tearing did not affect the inelastic performance of this connection. Local flange buckling was also observed at 3.5% rotation, which occurred in the girder beyond the connection region. This suggests that the connection was strong enough to initiate significant yield in the girder flange. Failure of this connection was due to fracture of the deformed bars at approximately 5.0% rotation. Three of the four bars failed by tension rupture, while one bar pulled out of the concrete core. No significant stiffness or strength deterioration
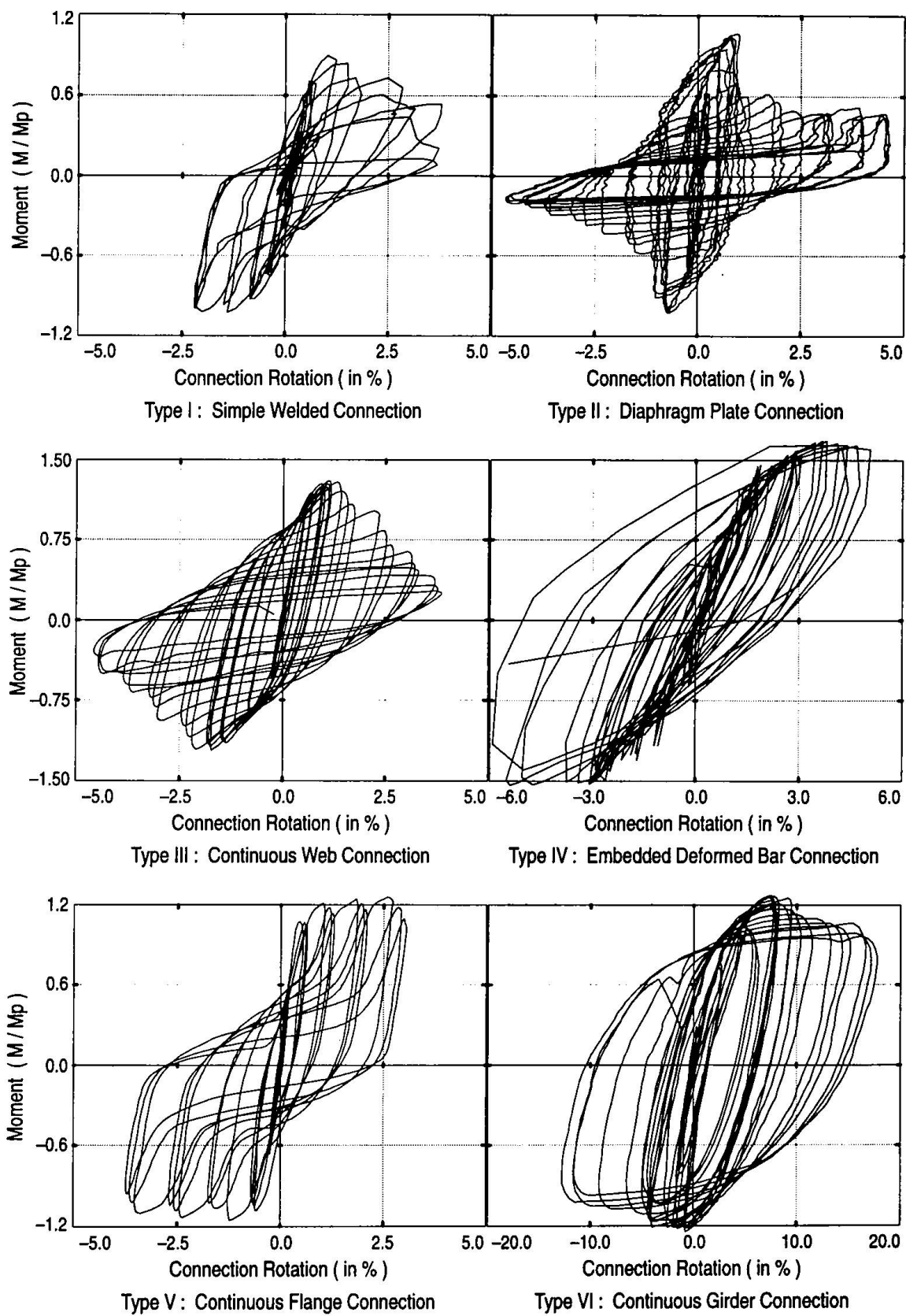
Figure 2. Experimental Moment–Rotation Behavior of Each Connection

was observed prior to the fracture of the deformed bars. Each deformed bar that failed in tension ruptured between the tube wall and the first weld location attaching the bar to the girder flange.

The *Type V* connection detail was tested to study the effect of continuing only the flanges through the CFT column. Flange plates were welded to the tube wall on each side of the column to transfer girder flange forces. The resistance was to be provided by bearing of the steel tube against the concrete core as needed. No attempt was made to enhance the bond between the embedded plates and the concrete core. The lack of bond impacted the hysteretic performance of this connection significantly compared to the other connection types. Both flange welds on the girder side of the column connection fractured at approximately 0.5% rotation. The flange welds on the column-side opposite the girder remained in tact. This caused the flanges to push through the concrete core resulting in fracture of the steel tube. This tube wall fracture initiated at approximately 1.0% rotation. As new deformation amplitudes were reached the connection resistance increased, but this resistance diminished upon subsequent cycles. This resulted in excessive pinching of the hysteretic behavior.

Results for connection *Type VI* exhibited quite stable inelastic behavior. Local flange buckling was observed at approximately 4.0% rotation, and web buckling was observed at about 5.0% rotation. Deterioration of the inelastic characteristics were observed after the onset of the local web buckling. This connection was clearly able to develop the plastic bending strength of the girder. Failure of this connection was due to fracture of the beam flange in the connection stub region. This flange tearing eventually propagated into the web. Although the flexural strength decreased approximately 30% compared to the peak value, hysteretic behavior remained stable even at very large rotations. After the test, the steel skin was removed from the concrete core in the region around the connection. No crushing of the concrete core was observed, and the tube wall showed no apparent signs of distress.

3. Conclusions

In general, inelastic connection behavior improved significantly when a larger portion of the girder force was transferred to the concrete core. However, the inelastic performance depended significantly on the connection detail. Some conclusions from this study are worth noting:

1. Connection *Type I* could not develop the plastic bending strength of the girder, while the flange, weld, and tube wall were susceptible to fracture. This connection lost almost all of its flexural strength at moderate inelastic demands. This connection should not be used in moment-resisting frames in regions of moderate to high seismic risk.

2. Connection *Type II* was able to develop the yield strength of the girder, however, the inelastic properties deteriorated rapidly at the onset of the diaphragm fracture. This connection might be used in low to moderate seismic zones.

3. Extending the web through the connection, as in detail *Type III*, improved the inelastic performance of the simple connection. However, the *Type III* connection still experienced significant web tearing and an eventual deterioration of the shear capacity. Partially embedded shear tabs may offer more favorable shear resistance for the girder if the flanges or steel tube skin fracture.

4. Weldable deformed bars transferred much of the flange stresses into the concrete core. This connection showed considerable improvement over simple connection *Type I*, and could be used in regions with moderate to high seismic activity.

5. Continuing flange plates, as tested in connection *Type V*, did not produce satisfactory inelastic, cyclic behavior. The inability of the weld to transfer flange forces to bearing stresses to the concrete core on either side of the connection resulted in large deformations with little resistance unless a new deformation amplitude was imposed. This produced a significantly pinched hysteretic behavior.

6. The *Type VI* through connection exhibited favorable hysteretic behavior. This appeared to be the most effective method to develop the plastic bending strength of the steel girder, and was closest to representing ideal rigid connection conditions. While there appeared to be a 30% flexural strength decrease, the subsequent flexural resistance was equivalent to the plastic bending strength of the girder. Further, the cyclic behavior remained stable even at very large rotations.

Acknowledgments

References

ATC-24 (1992). Guidelines for Cyclic Seismic Testing of Components for Steel Structures. *Applied Technology Council*. Redwood City, CA.

Azizinamini, A. and Prakash, B. (1993). A Tentative Design Guidelines for a New Steel Beam Connection Detail to Composite Tube Columns. *AISC Engineering Journal*, 3rd quarter, 108-115.

Ansourian, P. (1976). Connections to Concrete-Filled Tube Columns. *International Association of Bridge and Structural Engineers*, **36-I**, 1-22.

Bridge, R. and Webb, J. (1992). Thin Walled Circular Concrete Filled Steel Tubular Columns. *Composite Construction of Steel and Concrete II, ASCE*, 634-649.

Kanatani, H., Tabuchi, M.. Kamba, T., Hsiaolien, J., and Ishikawa, M. (1987). A Study on Concrete Filled RHS Columns To H-Beam Connections Fabricated with HT Bolts in Rigid Frames. *Composite Construction of Steel and Concrete, ASCE*, 614-635.

Kato, B., Kimura, M., Ohta, H. and Mizutani, N. (1992). Connection of Beam Flange to Concrete-Filled Tubular Columns. *Composite Construction of Steel and Concrete II, ASCE*, 528-538.

Morino, S., Kawaguchi, J., Yasuzaki, C., and Kanazawa, S. (1992). Behavior of Concrete Filled Steel Tubular Three Dimensional Subassemblages. *Composite Construction of Steel and Concrete II, ASCE*, 726-741.

Prion, H.G.L., and McLellan, A.B. (1992). Connecting Steel Beams to Concrete-Filled Steel Columns. *In Proceedings, ASCE Structures Congress on Composite Compression Members*, San Antonio, TX, 918-921.

Shakir-Khalil, H. (1992). Full Scale Tests on Composite Connection. *Composite Construction of Steel and Concrete II, ASCE*, 539-554.

Valbert, G. (1968). Essais d' Assemblages Soudes d'une Solive Sur un Poteau en Tube Rempli de Beton. *Construction Metallique*, 4 Dec., 27-38. (in French).

Low-Cycle Behaviour and Analysis of Steel-Concrete Composite Substructures

Oreste BURSI
Research Associate
Univ. di Trento
Trento, Italy

Oreste Bursi, born 1959, received
his Mechanical Engineering
Degree at the University
of Padua, Italy. Since 1986,
he has been at the University
of Trento. His research interest
is devoted to elastodynamics,
structural plasticity as well
as analysis and modelling of
both steel and steel-concrete
composite structures.

Marco BALLERINI
Research Associate
Univ. di Trento
Trento, Italy

Marco Ballerini, born 1960, got his
Civil Engineering Degree at the
University of Pavia, Italy. Since 1989,
he joined the University of Trento. His
research interest concerns the behaviour
of steel and timber connections as well
as the performances of steel-concrete
composite members under alternate loading.

Summary

Tests and analyses of steel-concrete composite structures subjected to alternate loads are proposed as part of an investigation on aseismic design of composite systems. Hence, quasi-static cyclic and pseudo-dynamic tests on composite beams with full and partial shear connection as well as complementary monotonic and cyclic tests on pull-push specimens were carried out. Moreover, two-dimensional finite element analyses based on smeared-crack formulations including discrete stud connectors and bond were performed. The paper presents some significant results to date.

1. Beam-Column Substructures

The partial action between concrete deck and steel girder within composite framing systems in earthquake prone zones can provide more choice for the designer and may reduce costs. However, the assessment of frame performance with partial shear connection (PSC) composite beams requires beam finite elements embodying complex hysteresis analytical models. So far, few relevant experimental data on PSC beams subjected to low-cycle alternate loading are available.

1.1 Test Subassemblages, Procedures and Results

Four among six full scale composite beam specimens with PSC and full shear connection (FSC) were built and tested by Bursi and Ballerini [1]. According to EC-4 [2], a conventional degree of shear connection N/N_f equal to 0.68 and 1.32 was estimated for the PSC and FSC beam, respectively. The two companion PSC beams characterised by a N/N_f ratio of 0.45 are under testing. The geometrical characteristics of the composite substructures as well as part of the measurement apparatus are highlighted in Fig. 1. The beam axial displacement is detected by means of an external LVDT at the steel beam centroid whilst the slip between the steel beam and the composite slab is collected by means of coupled LVDTs located at Sections 1-4. Other related information are collected in [1]. Quasi-static cyclic lateral displacements were applied to the specimens according to the ECCS procedure [2] as implied by Fig. 1, whilst pseudo-dynamic tests were performed on companion specimens according to the test set-up highlighted in Fig. 2.

For conciseness, only some results are presented in what follows. The hysteresis loops of the reaction force developed by the FSC substructure *versus* the controlled displacement are plotted in Fig. 3a. The inelastic hysteretic behaviour exhibited by the specimen is governed by steel beam yielding for positive (pull) loads and rebar yielding as well as concrete fracturing for negative (push) loads. Web and flange buckling occurred at the first negative hemicycle characterised by a
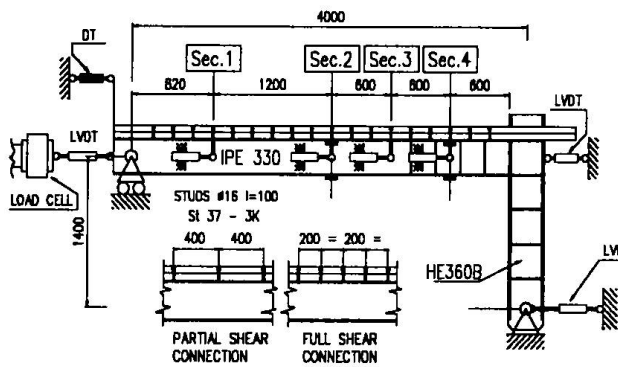
Fig. 1 Lay-out of substructure with full shear connection and relevant measurement apparatus
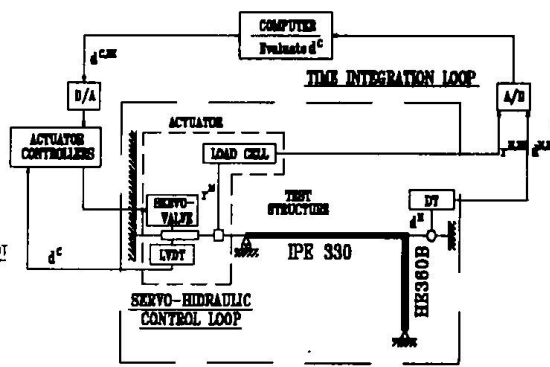
Fig. 2 Lay-out of the pseudo-dynamic test set-up
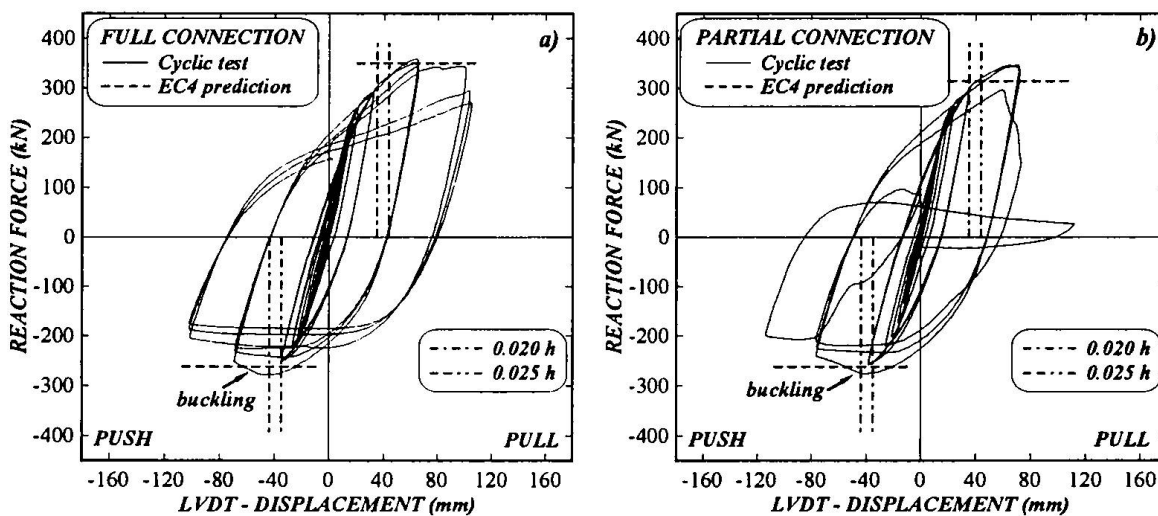
Fig. 3 Cyclic hysteresis loops of reaction force vs. controlled displacement of substructure with:
a) full shear connection; b) partial shear connection

Fig. 4 Pseudodynamic hysteresis loops of reaction force vs. controlled displacement of substructure with:
a) full shear connection; b) partial shear connection

displacement ductility factor of 4. In this respect, if one considers the interstorey drift limits corresponding to the ultimate limit state, 2.0%, as well as to the demolition state, 2.5%, respectively, under the assumption of a storey height of 3.5 m, the specimen behaviour appears to be satisfactory. The mean reaction force without safety factors as predicted by EC-4 [2] and corresponding to the maximum resistance of the composite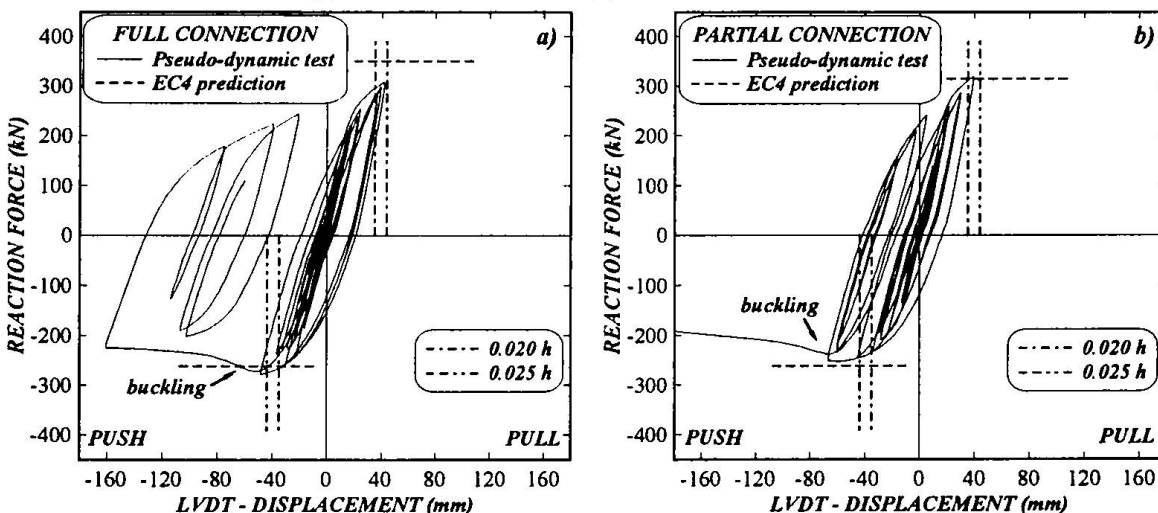 beam, is indicated in Fig. 3a. One can observe the shortcoming of EC-4 prediction when cyclic loads are involved. The corresponding reaction force-displacement loops germane to the PSC substructure are reported in Fig. 3b. Even in this test, web and flange buckling revealed at the first hemicycle with a displacement ductility factor of 4 whilst at the third positive hemicycle weld beads between the beam bottom flange and the column fractured. Nevertheless, the arguments posed in favour of the FSC substructure render the PSC substructure behaviour quite admissible. In order to grasp the behaviour of the aforementioned substructures with respect to random variable amplitude displacements some pseudo-dynamic test results are commented upon. The reaction force-displacement responses corresponding to the N69W component of the 1952 Taft earthquake, applied with a peak ground acceleration of 2.0g are mirrored in Fig. 4a and 4b for FSC and PSC substructure, respectively. One can observe an acceptable behaviour of the specimens up to the interstorey drift limits. Soon after, local instability phenomena reduced the energy consumption characteristics of specimens. Moreover, the energy absorption properties of specimens under pull loading were not exploited.

1.2   Finite Element Model and Analyses

The three-dimensional (3D) finite element modelling of PSC beams poses several problems due in part to the lack of interface material properties as well as in part to general computational difficulties. Thereby, a 2D finite element model that retains the most significant facets of the actual composite substructure was conceived by Bursi and Gramola [4]. Such a model is represented in Fig. 5 and it includes the following characteristics, among others: (*i*) discrete connectors with finite head dimensions, in order to reproduce the actual compressive stress state in the concrete deck; (*ii*) discrete reinforcing steel bars; (*iii*) overlapped nodes in order to simulate both structural and reinforcing steel-concrete interfaces. In this on-going investigation, elastic-plastic plane-stress simulations are performed on the test substructures by means of the concrete constitutive models available in the ABAQUS code [5]. In these models, a macro-level approach is adopted for concrete fracture and the plain concrete is assumed to be an equivalent isotropic continuum with smeared cracks. Longitudinal steel reinforcements in the composite deck were considered made of an hardening elastic-plastic material and were modelled either as *discrete* two-noded truss elements or as *smeared* overlay on top of smeared-crack elements. In the case of *discrete* reinforcements, the yield criterion for concrete was assumed to be an elastic-plastic model with strain-hardening based on the Drucker-Prager yield surface with a non-associated flow rule. When *smeared* reinforcements were adopted, the rebar-concrete interaction in the tensile stress regime was modelled implicitly by appropriate modifications of the constitutive relations of concrete. In such conditions, a more sophisticated inelastic concrete model embodied in the ABAQUS code [5] was adopted. In order to reduce the analysis complexity, only monotonically increasing loading is considered. As a result, some low-cycle degrading phenomena are neglected and the monotonic responses are assumed to be the skeleton curves. Moreover, only comparisons among test data and analyses relative to the FSC substructure in the predominant compressive stress state (pull loading) are discussed. In order to capture friction effects between the structural steel (beam upper flange and stud connectors) and the concrete, two limiting cases are analysed: full slip (low friction) and full stick (high friction) conditions. Relevant results are reported in Fig. 6a and, as expected, local friction effects appear to be not so significant. Substructure performances are analysed when *discrete* reinforcing bars are embodied into the model, *i.e.* when the bond stress-slip relationships are taken into account. In addition, the full slip condition was considered whilst the stud shear connectors were replaced with horizontal discrete springs characterised by hardening elastic-plastic constitutive laws obtained via pull-push
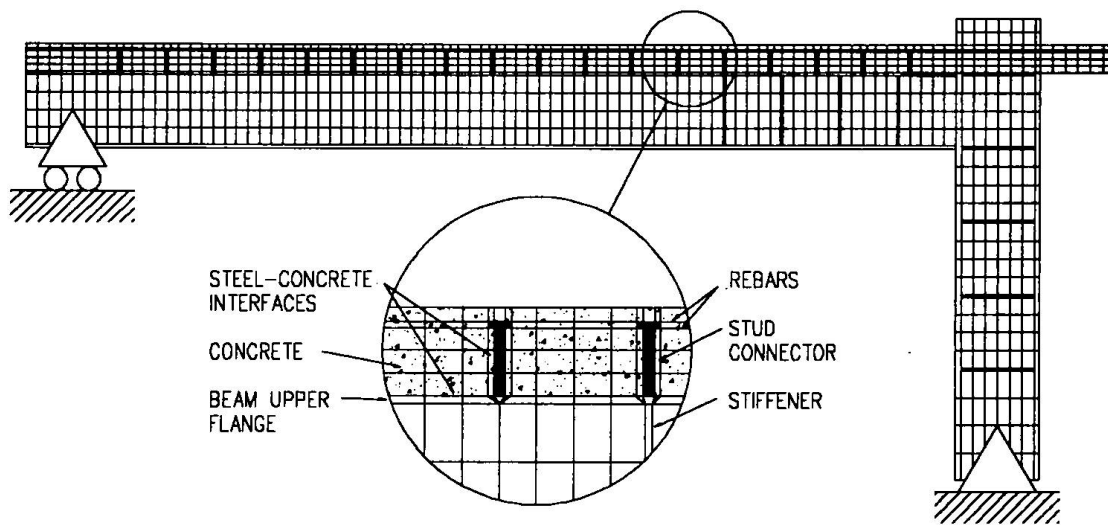
Fig. 5 Refined two-dimensional finite element model of substructure with full shear connection
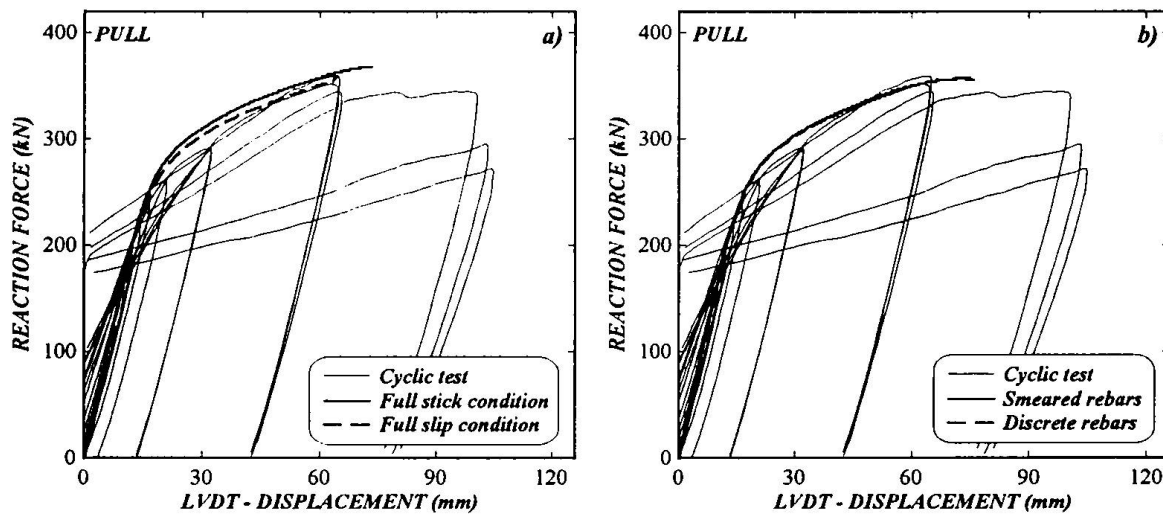
Fig. 6 Experimental and numerical results for full shear connection substructure:
a) smeared rebars; b) non-linear spring connectors
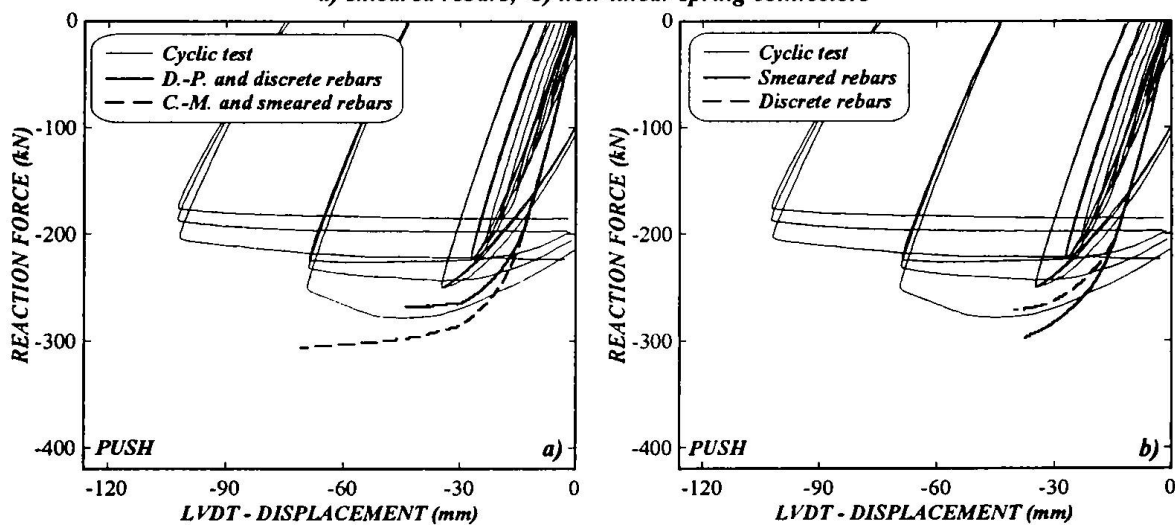
Fig. 7 Experimental and numerical results for full shear connection substructure:
a) Drucker-Prager (D.-P.) and Concrete-Model (C.-M.); b) non-linear spring connectors
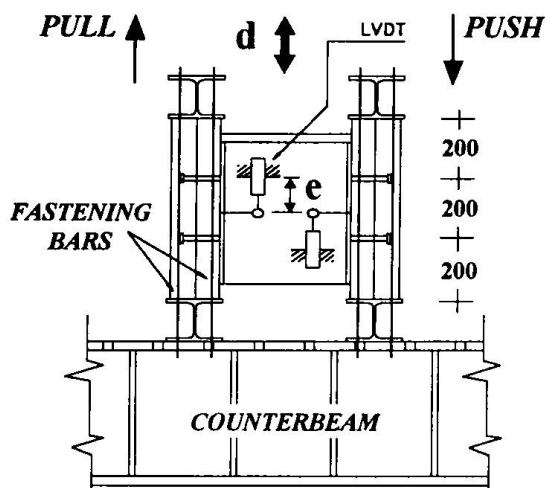
Fig. 8 Schematic lay-out of pull-push specimens

CYCLE NUMBER
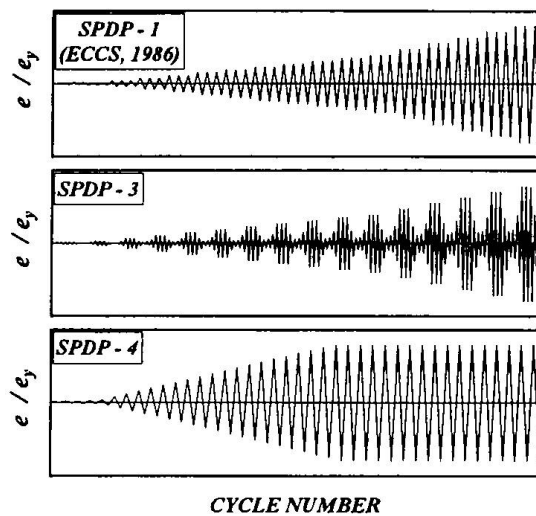
Fig. 9 Sequencial-phased displacement
test procedures
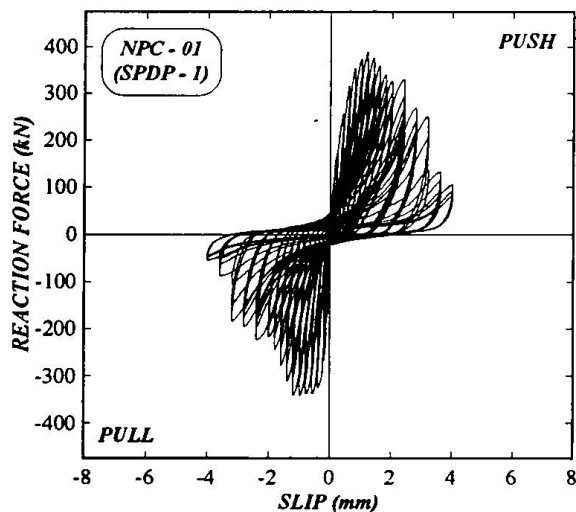
Fig. 10 Hysteresis loops of reaction force vs.
controlled slip of specimen NPC-01
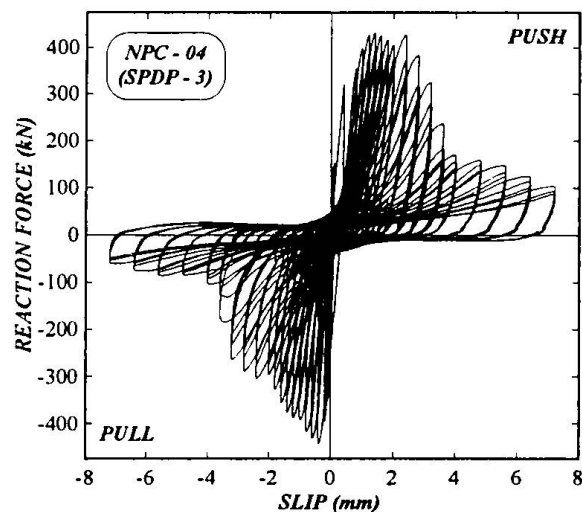
Fig. 11 Hysteresis loops of reaction force vs.
controlled slip of specimen NPC-04
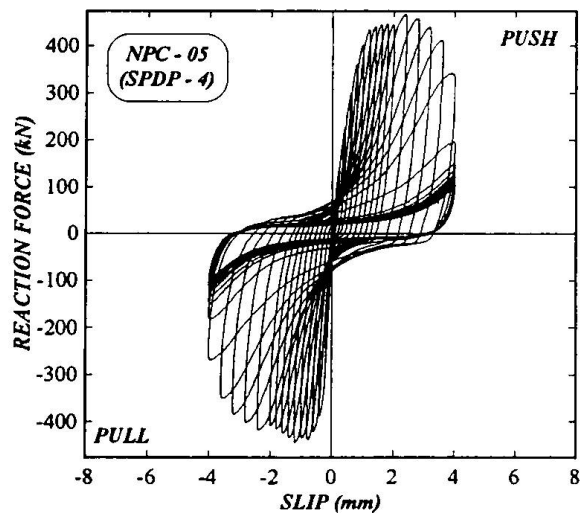
Fig. 12 Hysteresis loops of reaction force vs.
controlled slip of specimen NPC-05
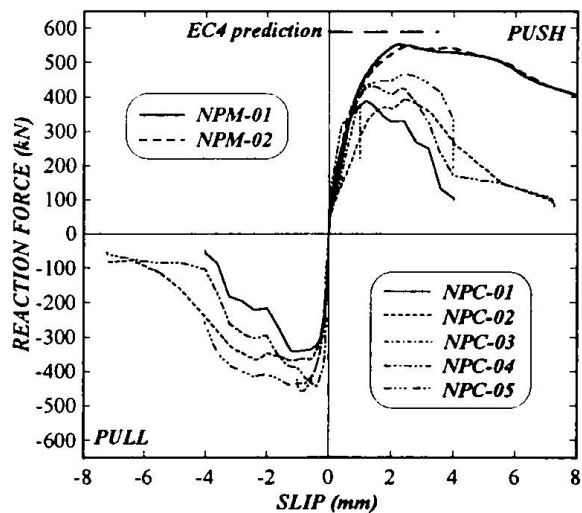
Fig. 13 Primary and skeleton curves of reaction
force vs. controlled slip of pull-push specimens

tests [1]. In order to suppress uplift, scleronomic constraints were imposed between the beam upper flange and the concrete deck. As a matter of fact, the overall simulated response highlighted in Fig. 6b is affected slightly by the bond stress-slip behaviour, owing to the predominant deck compressive stress state. Moreover, the high shear connection degree ($N/N_f = 1.32$) mitigates the effects caused by the presence of discrete springs. Nevertheless, the simulated responses result less strong because the confining effect exerted by the stud connector heads is lost. In a similar fashion, analyses were repeated for the stress regime characterised by the deck in tension. In this context, the bond stress-slip relationships have a significant bearing on the substructure strength as mirrored in Fig. 7a and these effects appear to be independent from the shear connection degree [4]. A similar trend persists even though discrete springs reproduce the actual stud shear connector responses as mirrored clearly in the simulations plotted in Fig. 7b.

2. Pull-Push Specimens

In order to expand the experimental data base and to calibrate finite element models for concrete-stud connector interaction, eleven customary pull-push specimens were tested in two series. For brevity, only some results germane to the second test series are commented here. The geometrical characteristics of these specimens are identical to those of the composite beams whilst the test specimen and set-up are plotted in Fig. 8, schematically. The relative slip e depicted in the same figure was assumed to be the prime parameter of test control. Some of the displacement histories are summarised in Fig. 9. In detail, the displacement procedures comprise both variable and constant sequential-phased displacement histories to impose different cumulative damages on the specimens. The reaction force-slip response of the NPC-01 specimen is highlighted in Fig. 10. The observed inelastic behaviour is caused by stud connector yielding and concrete fracturing whilst the specimen collapse was governed by concrete crushing. The stiffness and strength degradation in the range of the maximum load is limited. The corresponding cyclic response of NPC-04 specimen is plotted in Fig. 11. One can observe an increase of both strength and ductility properties of the specimen. The hysteretic behaviour of the NPC-05 specimen is shown in Fig. 12. The specimen was able to develop large reaction forces at large displacement ductility factor as a consequence of the displacement procedure SPDP-4 characterised by only one cycle per variable amplitude. Finally, the primary load-slip relationships provided by two specimens tested in a monotonic regime as well as the skeleton curves of the other specimens are collected in Fig. 13. One can observe how reversed displacement cycles inflict to the specimen responses a reduction both of strength and ductility. The mean shear resistance predicted by EC-4 [2] without safety factors is depicted in the same figure. One can observe the unsafe prediction, specially owing to the detrimental effects of reversed displacements. The investigation of the low-cycle behaviour as well as the calibration of damage criteria for composite members deserve additional future studies.

Acknowledgements

References

[1] Bursi O.S. and Ballerini M., "Behaviour of a Steel-Concrete Composite Substructure with Full and Partial Shear Connection", Eleventh WCEE, Acapulco, (1996), Paper No. 771.

[2] Eurocode 4 - ENV 1994-1-1:"Design of Composite Steel and Concrete Structures-Part 1-1: General Rules and Rules for Buildings", European Committee for Standardisation (1992)

[3] Technical Committee 13, "Recommended Testing Procedures for Assessing the Behaviour of Structural Steel Elements Under Cyclic Loads", ECCS, (1986), No. 45.

[4] Bursi O.S. and Gramola G., "Smeared Crack Analyses of Steel-Concrete Composite Substructures", STESSA '97, Kyoto, (1997).

[5] ABAQUS - User's Manual, ver. 5.5, Vol. 1-2, Hibbitt, Karlsson & Sorensen Inc., (1996).

Prediction of Cumulative Damage in SRC Beam-Columns

Yasuhiro UCHIDA
Associate Professor
Kagoshima University
Kagoshima, Japan

Yasuhiko KOJO
Civil Engineer
Nishimatsu construction
Tokyo, Japan

Akito BOCHI
Research Student
Kagoshima University
Kagoshima, Japan

Summary

The critical axial force for convergence-axial displacement curves of SRC and RC beam-columns are proposed as a characteristic curves for repeated loading in order to predict the cumulative damage. Tests and analyses of SRC and RC beam-columns were carried out and it was found that the cumulative damage could be evaluated by the curves very well.

1. Introduction ·

Since the strong horizontal force occurred in earthquake often causes the cumulative damage such as the strength deterioration and the accumulation of deformation in structures and their members, the prediction of cumulative damage is needed in the aseismic design of structures. In this study, the characteristic curves of composite steel and reinforced concrete (SRC) beam-columns are presented experimentally and analytically, and a method of predicting convergence-divergence phenomena in accumulation of deformation of beam-columns is explained.

2. Evaluation of Cumulative Damage by Characteristic Curve for Cyclic Loading

The strength deterioration and the accumulation of deformation in structures subjected to repeated loading are named cumulative damage in this study. Since the deteriorating behavior closely correlates with the accumulation of deformation, it is necessary to investigate the accumulation of deformation. A limit value of the axial force when the accumulation of deformation in a beam-column subjected to a repeated horizontal force converges to a certain value is named critical axial force for convergence. Since "critical axial force for convergence" is very long, it is termed "critical axial force" hereafter.

Procedures of obtaining the critical axial force of a beam-column are outlined as follows;
1) Give a value of converged axial displacement.
2) Apply an axial force so that the value of axial displacement may become a given value.
3) Apply a repeated horizontal force with a given constant displacement amplitude under the given axial displacement.
4) The minimum axial force obtained in the loading step 3) gives a critical axial force.
5) Increase the value of converged axial displacement and go to 1).

In general, the critical axial force is approximately given by the minimum value of axial force under an assumed axial displacement, because the varying axial force become a true one when it takes an extreme value, which can be derived from theorem of minimum potential energy. The relation between the critical axial force and the maximum of displacement varying in the converged state becomes the critical axial force-axial displacement relation.

## 3.   Critical Axial Forces of RC and SRC Beam-Columns

3.1   Experiments

3.1.1 Specimens and Mechanical Properties

RC and SRC specimens were tested under a axial force and a repeated horizontal force. Figure 2 exhibits the configuration and dimensions of SRC specimens, and those are same as ones of RC specimens except for the encased steel. Depth and width of SRC cross section are 150mm. In SRC specimens, an H-section of steel H-75x75x3.2x3.2 (mm) built up by welding is encased in concrete with 4 deformed main bars. Hoops of D6 are placed with a pitch of 50mm in bending failure type RC specimens and SRC specimens and with a pitch of 100mm in shear failure type RC specimens. Table 1 shows measured dimensions, compression strength of concrete, hoop ratio and spacing of hoops. The material properties of reinforced bars and steel are listed in Table 2. Specimens RC1~RC3 and SRC1~SRC2 are bending failure type specimens with hoop ratio $_wp=0.85\%$ and Specimens RC4~RC6 shear failure type ones with $_wp=0.43\%$.

3.1.2 Experimental Method

RC and SRC beam-columns under a repeated horizontal force and an axial force were tested. Figure 2 shows a test set-up. Specimens were fixed at its end horizontally to the loading frame because the height of the loading frame is not sufficient for erecting the apparatus vertically.
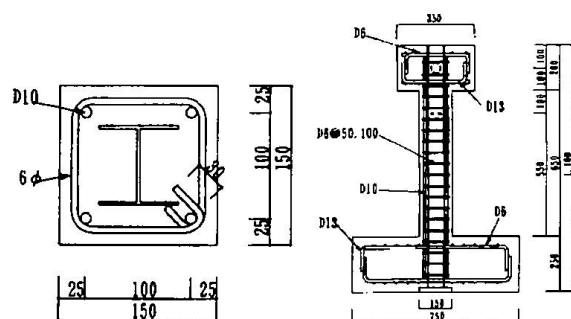
(a) Cross Section   (b) Elevation
Fig. 1 SRC specimen
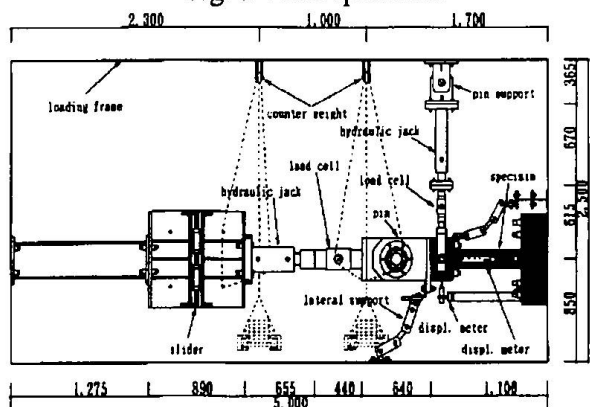
Fig. 2 Test set-up

Table 1 Exprimental Parameters

Spec. No.	B (mm)	D (mm)	ℓ (mm)	h (mm)	F_c 'kg/cm²	$_wp$ (%)	x (mm)
RC1	149.2	151.2	750.1	549.4	412	0.85	50
RC2	149.0	153.1	751.7	550.0	339	0.85	50
RC3	150.1	152.1	751.0	548.7	407	0.85	50
RC4	150.6	150.5	749.7	549.9	446	0.43	100
RC5	150.3	150.6	750.6	549.3	401	0.43	100
RC6	151.7	151.6	749.2	549.1	420	0.43	100
SRC1	148.5	150.5	750.0	550.5	388	0.85	50
SRC2	149.0	149.8	748.3	552.5	378	0.85	50

B=width, D=depth of cross section
ℓ =length, F_c=compression strength
$_wp$=hoop ratio, x=spacing of hoops

Table 2 Material properties

Materials		σ_y (t/cm²)	σ_u (t/cm²)	δ (%)
Re-Bars	D-6	3.96	6.11	18.4
	D-10	3.56	5.22	20.2
	D-13	3.44	5.02	19.4
Steel H-75x75x3.2x3.2		3.73	4.6	20.6

σ_y=yield stress, σ_u=tensile strength
δ=elongation

Repeated horizontal force with a constant displacement amplitude of 10mm was applied to the top of the beam-column by a hydraulic jack and an axial force was also applied to that through a pin. Here the horizontal force means the force in the direction perpendicular to the axial direction of the specimen. The hydraulic jack for axial loading was attached to a slider so that the axial compressive and tensile force can be applied with moving.

Critical axial forces were obtained by two kinds of loading. To Specimens RC2 and RC5, a repeated horizontal force was applied in three cycles successively with keeping the axial displacement constant (Test 1). The critical axial force can be given by the minimum value of the axial force in the third cycle. In Specimens RC3 and RC4, critical axial forces were obtained by providing the variable axial displacement assumed on the base of displacement in the previous step (Test 2). The convergence-divergence behavior of axial deformation was investigated under an axial force varied in the stepwise manner in the vicinity of the critical axial force-displacement relation in order to verify the validity of the critical axial force obtained by Test 1 and Test 2. The horizontal displacement δ_h at the top of specimens was measured by a displacement meter installed on the stand and the axial displacement δ_v by displacement meters equipped on sliders set up between both ends of the specimen. The measured displacement δ_v is, however, not a vertical displacement but a displacement in the axial direction of the specimen.

3.13 Test Results and Discussions

Figs. 3 through 9 exhibit test results of RC and SRC specimens. The axial force p-axial displacement δ_v relations of Specimens RC2 and RC5 is shown in Fig. 3 where open squares represents the maximum point of varying axial force-minimum axial displacement, and open circles the minimum point of varying axial force-maximum axial displacement. Figure 3(a) is a result for bending failure type specimens and Fig. 3(b) for shear failure type specimens. p in these figures is the axial force normalized by $F_c BD$ in which F_c denotes compressive strength, and B and D denote width and depth of the cross section. Open circles and solid circles in Figs. 4(a) and (b) indicate the axial force p-axial displacement δ_v relations of bending failure type Specimen RC1 and shear failure type Specimen RC6 subjected to a constant axial force in a stepwise manner. The solid line in these figures indicate the critical axial force-axial displacement relation expressed by the inner curve formed by curves with open squares and open circles. The stages of constant axial force loading are designated by 1~10 and 1~8. Open circles and solid circles in the loading stage represents convergence and divergence in the accumulation of deformation, respectively. Figs. 5 and 6 show the critical axial force-axial displacement relation and the accumulation of deformation under a constant axial force for Specimens SRC1 and SRC2. The axial force of SRC specimens is normalized by the axial ultimate strength $\{ _cy_u F_c BD + _s A _s\sigma_y + _r a _r\sigma_y \}$ where $_r\sigma_y$=yield stress of reinforced bar, $_cy_u$=0.85-2.5$_sp_c$, $_sp_c = _sa_c/BD$, $_sa_c$=area of a steel flange, $_s\sigma_y$=yield stress of steel, $_sA$=area of the encased steel, $_ra$=total area of reinforced bar.

Figures 7(a) and (b) are horizontal force h-horizontal displacement δ_h relations for bending failure type Specimens RC1 under constant axial forces p=-0.18 (loading stage 3 in Fig. 4 (a)) and -0.26 (stage 4), and Figs. 8(a) and (b) for shear failure type Specimens RC6 under constant axial forces p=-0.33 (stage 4 in Fig. 4(b)) and p=-0.41(stage 5). Hysteresis loops of Specimen SRC2 under p=-0.17(stage 3 in Fig. 6) and p=-0.23 (stage 4) are shown in Fig. 9(a) and (b), respectively. Horizontal force h of RC and SRC specimens are normalized by ultimate strengths $\{ a_t\sigma_y(D-2d_c)+0.12BD^2F_c \}/\ell$ and $\{ _cy_u bD^2 F_c/8 + _sZ_p\sigma_y + a_t\sigma_y (D-2d_c) \}$ prescribed in A.I.J standards, respectively, where a_t=total area of tension reinforced bars, d_c=depth of cover concrete, ℓ=length of specimen, $_sZ_p$=plastic section modulus of steel.

The accumulation of deformation converges and the hysteresis loop closes in the beam-column under a axial force less than the maximum critical axial force (Figs. 3 through 9). In the beam-column under a axial force greater the maximum critical axial force, however, the cumulative damage increases with the divergent accumulation of deformation and strength deterioration due to bending failure or shear failure. Figures 3 through 9 show that the critical axial force p_{cr}-axial displacement δ_v relation forms a hysteresis and the strength deterioration and the accumulation of deformation increase with the increase in the slope of the descending p_{cr}-δ_v curve. Therefore, it is noted that the progress of strength deterioration and the convergence-divergence behavior in

the accumulation of deformation are predictable by p_{cr}-δ_v curves.
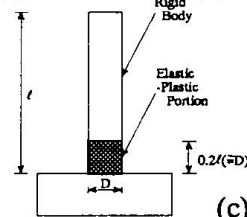
3.2 Analyses

Analytical models of SRC beam-columns are shown in Fig. 10. Models of RC beam-columns are identical with that of SRC beam-columns except for the encased steel. Cross sections of models are divided into a number of segments and are idealized in Model A (Fig. 10(a)) of the gross cross section and Model B (Fig. 10(b)) of cross section without cover concretes in consideration of spalling due to compression. Fig. 10(c) exhibits the analytical model of beam-columns which consists of an elastic-plastic portion and a rigid body. The length of the elastic-plastic portion is 0.2ℓ and is the depth of cross section D approximately, where ℓ is the length of beam-column. Figures 11(a) and (b) show an assumed stress-strain relation of the reinforced bar, steel and concrete, in which the tension is taken positive. Stress 's' of concrete is normalized by compression strength and stresses of reinforced bar and steel are normalized by yield ones. Strains are also normalized in the same way as stresses. Skeleton curve of stress-strain relations of concrete are expressed as a function $f_1(e)$ as shown in Eq. (1). The strain e_u at the ultimate point of the stress-strain relation was assumed to be -3.
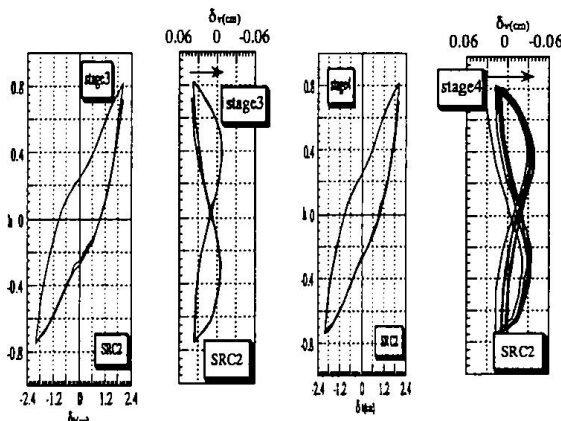
(a) p=-0.17, conv.　　(b) p=-0.23, div.
Fig. 9 Hysteresis loops of SRC beam-columns
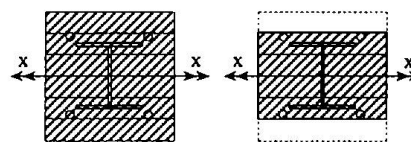
(a) Model A　　(b) Model B

(c) Beam-column
Fig. 10 Analytical models
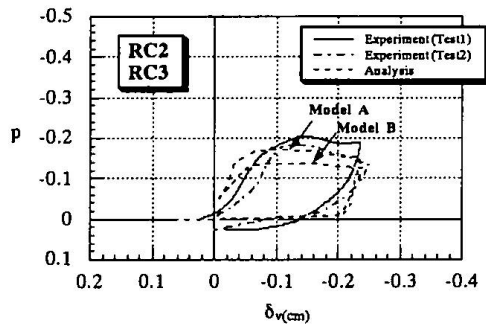
(a) RC (Bending failure type)
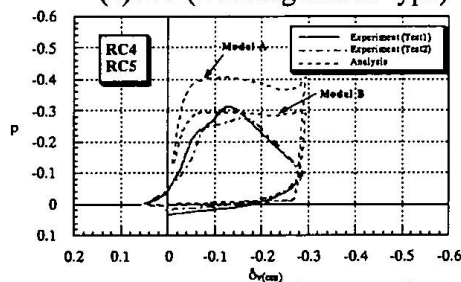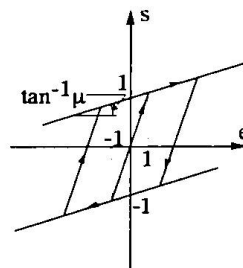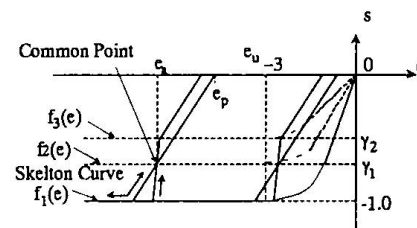
(a) Re-bars and steel　　(b) Cocrete
Fig. 11 Stress - strain relations
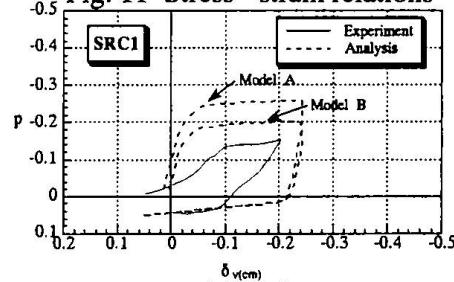
(b) RC (Shear failure type)　　(c)SRC

Fig. 12 Comparison between p_{cr} - δ_v curves obtained by tests and analyses
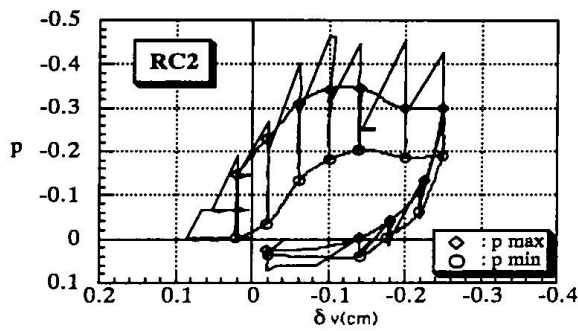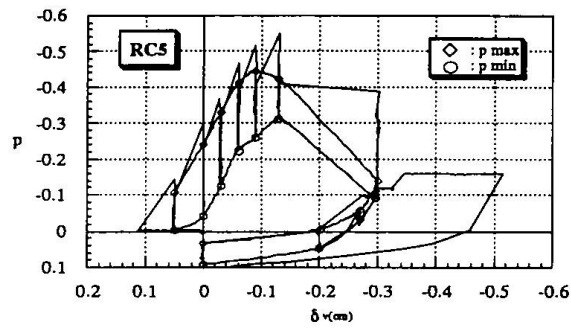
(a) Bending failure (b) Shear failure

Fig. 3 p_{cr} - δ_v curves of RC beam-columns
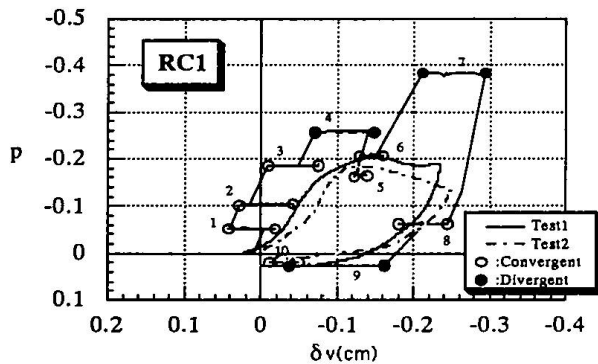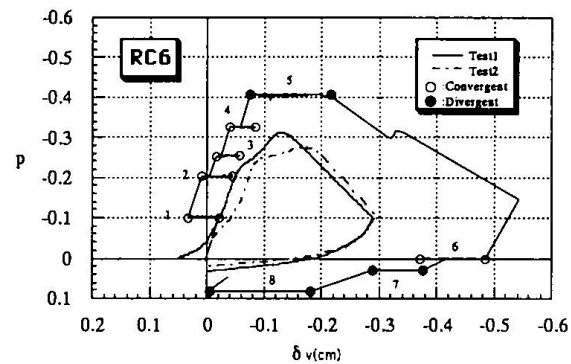
(a) Bending failure (b) Shear failure

Fig. 4 Prediction of cumulative damage of RC beam-columns
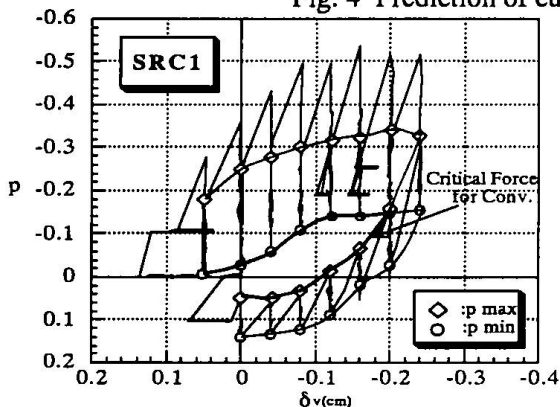
Fig. 5 p_{cr} - δ_v curves of SRC beam-columns
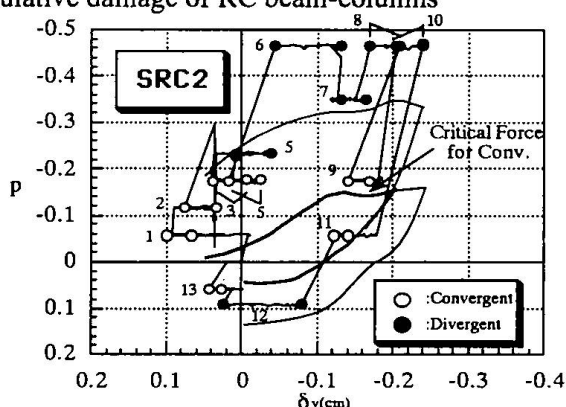
Fig. 6 Prediction of cumulative damage of SRC beam-columns
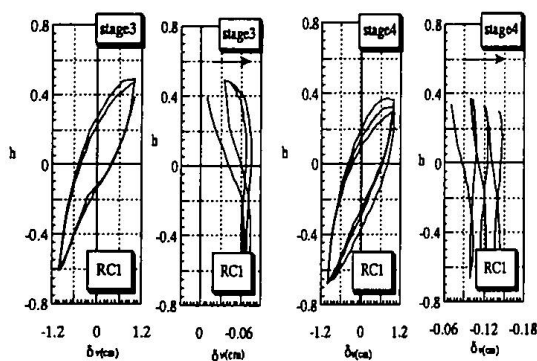
(a) p =-0.18, conv.   (b) p=-0.26, div.

Fig. 7 Hysteresis loops of RC beam-columns (Bending failure type)
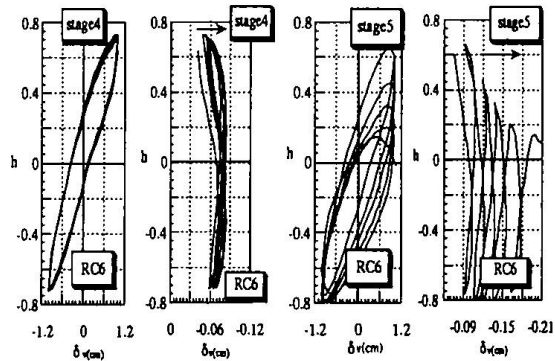
(a) p=-0.33, conv.   (b) p=-0.41, div.

Fig. 8 Hysteresis loops of RC beam-columns (Shear failure type)

$$f_1(e) = \frac{e}{1 - (1 + \frac{2}{e_u}) \cdot e + \left(\frac{e}{e_u}\right)^2} \quad \text{------ } e \geq e_u, \quad f_1(e) = -1 \quad \text{---------- } e < e_u$$

$$e_p = e_a \cdot \left(1 - e^{-\frac{1}{3}\left(\frac{e_a}{e_u}\right)^{1.5}} \right) \qquad f_2(e) = -\gamma_1 \cdot f_1(e) \qquad f_3(e) = -\gamma_2 \cdot f_1(e) \qquad (1)$$

where e_a=strain at a common point, e_p=plastic strain.

In this analysis, the critical axial force was obtained by using the axial displacement δ_v in the previous calculation step in the similar way to Test 2 in the experiment. Parameters listed in Tables 1 and 2 were used in analyses. Sections of concrete and steel were divided into 6 and 14 elements, respectively. Young's modulus of concrete and steel were assumed to be 210t/cm² and 2100t/cm², respectively. Coefficients related to degrading of the s-e relation of concrete as shown in Fig. 11(b) were chosen such that γ_1=-0.7, γ_2=-0.5 for RC beam-column, γ_1=-0.4, γ_2=-0.2 for SRC beam-column. Smaller coefficients of SRC beam-column were given in view of poor casting. The amplitude of displacement δ_{ha} was taken equal to 10mm. Eq. (2) is derived for the analytical model as shown in Fig. 10(c). The curvature at the base of beam-column can be given by Eq. (2) with the use of the displacement at the top of the beam-column δ_h. The bending moment and the horizontal force of a beam-column were also computed from the curvature Φ.

$$\frac{\Phi}{\Phi_y} = \frac{\delta_h}{\delta_{hy}} \qquad (2)$$

where Φ_y and δ_{hy} are Φ and δ_h at the yield point, respectively.

Critical axial force p_{cr}-axial displacement δ_v relations of RC and SRC specimens derived by analyses are shown in Fig. 11 in cases of Models A and B together with those by tests. p_{cr}-δ_v relations obtained by analyses mostly agree with test results.

4. Conclusions

1) Cumulative damage of SRC and RC beam-columns subjected to repeated horizontal loading can be predicted by critical axial force-axial displacement relation experimentally and analytically.

2) Critical axial force-axial displacement relation forms hysteresis. Limit point of the curve and the slope of the descending curve represents the resisting capacity of the beam-column for cumulative damage.

3) The critical axial force-axial displacement relation is useful for the limitation of axial force of SRC and RC beam-columns in order to keep the aseismic safety.

References

Architectural Institute of Japan (1987). AIJ Standards for Structural Calculation of Steel Reinforced Concrete Structures.
Uchida, Y. (1996). Estimation of cumulative damage of beam-columns and frames subjected to repeated loading, Proceedings of 11WCEE, CD-ROM.

Acknowledgment

Pseudodynamic Tests of Partially Concrete-Filled Steel Bridge Pier Models

Tsutomu USAMI
Professor
Nagoya University
Nagoya, Japan

Tsutomu Usami, born in 1943, graduated form Nagoya University in 1965. He received Doctor of Science Degree from Washington University in 1971, and Doctor of Engineering Degree in 1976. He has been actively engaged in research on steel and composite structures.

Hanbin GE
Assistant Professor
Nagoya University
Nagoya, Japan

Hanbin Ge, born in 1965, graduated from Huazhong University of Science and Technology, China, in 1986. He received Doctor of Engineering Degree in 1994 from Nagoya University. He has been engaged in research on steel and composite structures.
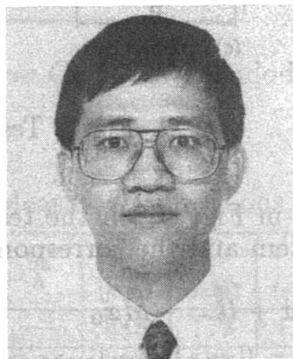
Kunihiro MORISHITA
Research Engineer
Mitsubishi Heavy Industry
Hiroshima, Japan

Kunihiro Morishita, born in 1971, graduated from Nagoya University in 1994. He received his Master Degree in 1996 from Nagoya University. He has been engaged in research and development on civil engineering structures such as bridge, chimney and crane.
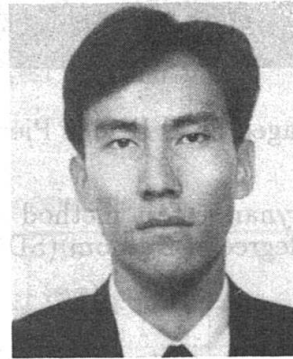
Summary

In the present paper, experimental results of concrete-filled steel box columns under dynamic loading are reported. To investigate the dynamic behavior of concrete-filled steel box columns, three specimens with different natural periods were tested using the pseudodynamic test method. For comparison, a hollow steel column specimen with the same dimension was also tested. Test results showed that concrete-filled steel box columns can be effectively used as bridge substructures to withstand severe earthquakes.

1. Introduction

Use of steel bridge piers becomes more and more popular especially in Japan. Steel bridge piers are normally designed as cantilever columns or planar rigid frames with thin-walled box or pipe sections. However, severe damage and even total collapse of such piers was observed during the Hyogoken-nanbu Earthquake on January 17, 1995. One such pier is shown in Fig. 1 where local buckling can be seen near the base. This shows the insufficient ductility capacity of the steel bridge piers to the strong earthquakes.

In order to study the seismic behavior of steel box columns and concrete-filled steel box columns under cyclic and dynamic loading, a large number of tests[1~3] have been carried out at Nagoya University since 1989. These studies produced a lot of valuable information in developing rational earthquake-resistant ultimate-strength design methods for such bridge piers.

2. Outline of Pseudodynamic Tests

In this study, test specimens used are of box sections with with one or two stiffeners on each flange plate and one stiffener on each web plate (see Fig. 2). A conceptual flow of
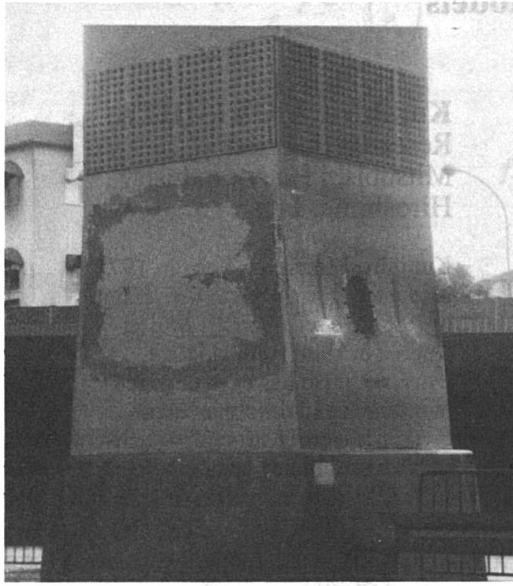
Fig. 1 Damaged Steel Bridge Pier
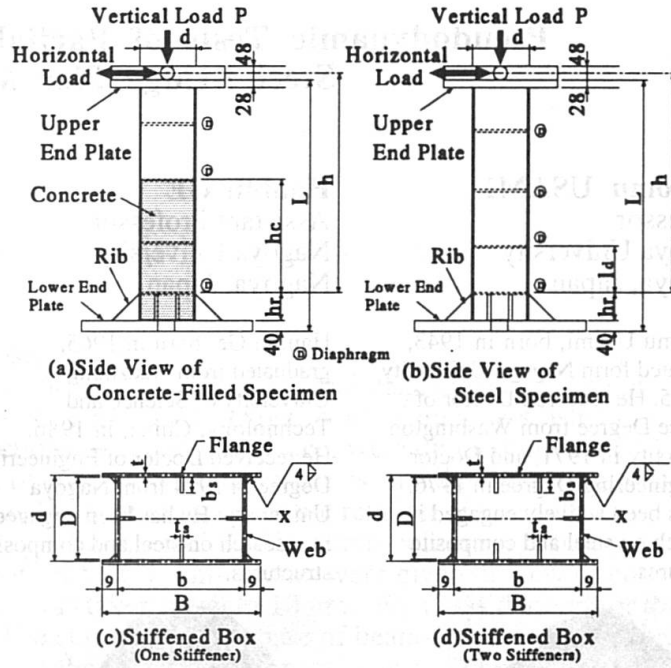
Fig. 2 Test Specimens

the pseudodynamic test method is shown in Fig. 3. In the test the specimen is modeled as a single-degree-of-freedom (SDOF) system and the corresponding equation of motion is solved.

$$M\ddot{x} + C\dot{x} + R = -M\ddot{x}_0 \tag{1}$$

The mass M of the system is calculated according to the Japanese Road Association code[4] in which the weight of a superstructure and 80 % of the weight of the bridge pier are considered. The damping coefficient C is then obtained from the mass and stiffness K with a value of 0.05 for the damping factor ξ. The ground motion accelerogram $\ddot{x}_0$ is specified in the form of a digitized record for each time step. In each step, a specified displacement is quasi-statically applied to the specimen, and the corresponding restoring force R induced is measured and used to compute the displacement to be imposed in the next step. The equation of motion is solved using an explicit integration method.

Although many factors may affect the seismic response of the bridge pier, discussion will now be limited to the effects of the filled-in concrete and natural period. For this purpose, one steel specimen and three concrete-filled steel specimens are designed and tested as cantilever type of columns fixed at the base. A scale factor of $S = 8$ was used in fabricating the specimens.[5] The measured dimensions of the specimens are given in Table 1. In the table, R_f and $\overline{\lambda}$ are flange width-thickness ratio parameter and column slenderness ratio parameter, respectively, and defined by

$$R_f = \frac{b}{nt}\sqrt{\frac{12(1-\nu^2)}{\pi^2 k}}\sqrt{\frac{\sigma_y}{E}} \quad , \qquad \overline{\lambda} = \frac{Kh}{r}\frac{1}{\pi}\sqrt{\frac{\sigma_y}{E}} \tag{2,3}$$

in which b = flange width; t = plate thickness; n = number of panels of a flange; σ_y = yield stress; E = Young's modulus; ν = Poisson's ratio; k = buckling coefficient of plate panel = 4.0; h = column height; K = effective length factor (= 2.0 for a fixed-free column); and r = radius of gyration of steel section.

From the tension tests of three coupons, average material properties of steel are determined and shown in Table 2. The average material properties of concrete are $f_c = 19.4$ MPa, $E_c = 22.3$ and $\mu = 0.162$. The length of filled-in concrete determined is based on an optimum length concept used in a previous study.[6] The optimum length of filled-in concrete is such

Experiment

Applying X_{i+1} Using Actuator Control System

P X_{i+1}

R_{i+1}

Measure R_{i+1}

START

① Input Earthquake Wave ($\ddot{x}_0$)

Calculation

② Calculate Next Step Displacement X_{i+1} Using

$$M\ddot{x} + C\dot{x} + R = -M\ddot{x}_0$$

1)Linear Acceleration Method
   Displacement < 0.5mm

2)Central Difference Method
   Displacement ≥ 0.5mm

③ D/A Conversion of Displacement (x_{i+1})

④ Taking in Horizontal Load(R_{i+1})
   and Displacement(x_{i+1})
   A/D Conversion

$i+1 \rightarrow i$

STOP

Fig. 3 A Flow Chart for Pseudodynamic Test Method

Table 1 Measured Dimensions of Test Specimens

Specimen	L (mm)	h (mm)	$\frac{h_c}{h}$	B (mm)	D (mm)	t (mm)	bs (mm)	ts (mm)	γ/γ^*	$\bar{\lambda}$	R_f
S45-35H	1153	973	—	285	172	4.31	42	4.31	14.1	0.380	0.480
SC45-25-25H	1051	904	0.25	321	197	5.00	43	5.00	2.4	0.262	0.404
SC45-35-20H	1449	1265	0.20	321	197	4.71	43	4.71	2.7	0.374	0.436
SC45-60-20H	1653	1434	0.20	220	130	5.05	30	5.05	2.3	0.619	0.400

Note: γ = relative flexural rigidity of one stiffener;
γ^* = Optimum value of γ obtained from linear buckling theory;
For other notations, refer to Fig. 2.

a value that makes both the hollow steel section and concrete-filled steel section near the column base reach simultaneously failure. At this state, the ductility of the column will be highest.

The axial loads used in the tests were calculated based on the expected horizontal force given by the seismic coefficient of the Japan Road Association code[4] and the interaction equations proposed by Usami.[7] The calculated values of the axial loads for the specimens are shown in Table 3.

Table 2 Material Properties of Steel

Specimen	σ_y (MPa)	E (GPa)	ν
S45-35H	374	192	0.277
SC45-25-25H	295	208	0.266
SC45-35-20H	303	207	0.263
SC45-60-20H	295	208	0.266

Three earthquake accelerograms (JMA, JR-Takatori and Higashi-Kobe) recorded during the Hyogoken-nanbu Earthquake of January 17, 1995 were used. The accelerograms are shown in Fig. 4 and it should be noted that the records JMA, JR-Takatori and Higashi-Kobe were

Table 3 Input Values of Pseudodynamic Tests

Specimen	Ground Type	$\frac{P}{P_y}$	M $kN \cdot s^2/mm$	K kN/mm	C $kN \cdot s/mm$	T sec	$\frac{\delta_R}{\delta_y}$	$\frac{\delta_{max}}{\delta_y}$	$\frac{H_{max}}{H_y}$
	III	0.143	1.841	117.22	1.551	0.764	1.22	3.30	1.55
S45-35H	I	0.199	2.551	117.22	1.825	0.899	1.77	3.75	1.78
	II	0.167	2.139	110.81	1.620	0.873	5.34	10.61	1.70
	III	0.172	2.148	327.03	2.650	0.509	0.10	2.40	1.52
SC45-25-25H	I	0.235	2.931	289.06	2.911	0.635	2.18	9.52	2.24
	II	0.199	2.479	267.70	2.576	0.605	1.43	10.12	2.24
	III	0.130	1.561	108.95	1.304	0.752	0.90	3.42	1.80
SC45-35-20H	I	0.182	2.177	99.46	1.471	0.929	1.17	4.44	1.94
	II	0.152	1.818	98.92	1.341	0.852	2.63	9.75	2.03
	III	0.081	0.655	23.19	0.390	1.056	0.89	3.03	1.49
SC45-60-20H	I	0.129	1.036	21.97	0.477	1.365	0.38	2.78	1.64
	II	0.096	0.770	20.75	0.399	1.211	0.44	5.43	1.79

obtained respectively from Ground Types I, II and III. Here, ground Types I, II and III correspond to hard (rock), medium and soft soil sites, respectively. The specimens were repeatedly subjected to these accelerograms in the order of Higashi-Kobe, JMA and JR-Takatori.

In Table 3, the values of the mass M, stiffness K, damping coefficient C and natural period T for converted real bridge piers ($S = 8$) are summarized. The natural period of each specimen, T, is computed as

$$T = 2\pi\sqrt{\frac{M}{K}} \qquad (4)1$$

3. Experimental Results

To investigate the effect of filled-in concrete on the seismic response of steel box columns, a steel specimen

Fig. 4 Input Earthquake Accelerograms

S45-35H and a concrete-filled steel specimen SC45-35-20H are considered here. As indicated previously, for the specimen SC45-35-20H, the length of filled-in concrete is determined as $0.2h$ based on the optimum length concept.

Fig. 5 shows horizontal displacement-time history and horizontal load-horizontal displacement curves obtained from the tests of the two specimens subjected to JR-Takatori accelerogram. The comparison shows the difference in the displacement response and restoring force. The measured residual displacement δ_R after the test and maximum displacement response δ_{max} during the test for each input accelerogram are summarized in Table 3. As can be seen from Fig. 5 and Table 3, the maximum response displacements δ_{max}/δ_y are almost the same but the residual displacement δ_R/δ_y is significantly reduced by filling concrete inside. For both accerelograms of JR-Takatori and JMA, the residual displacement of the concrete-filled
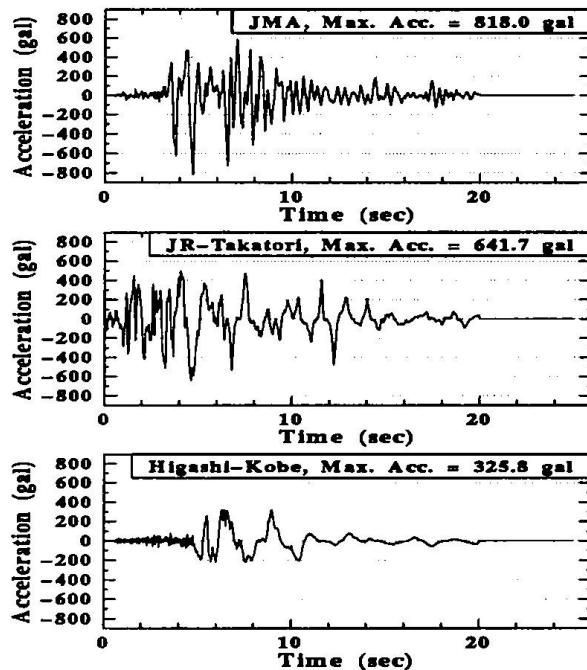
steel specimen SC45-35-20H is only about half of that of the hollow steel specimen S45-35H. Therefore, it can be concluded that the filled-in concrete is effective in improving the seismic behavior of steel columns. The damage appearance of the hollow steel specimen S45-35H after the test is shown in Fig. 6.

Three concrete-filled steel specimens are used herein to investigate the effect of the natural period on the seismic behavior of the columns. The specimens are of nearly the same values of R_f, but significantly different values of $\overline{\lambda}$. Thus, the natural periods of the specimens converted to real bridge piers with $S = 8$ are largely different. As an example, Fig. 7 shows time history responses and horizontal force versus horizontal displacement responses of the three specimens subjected to the JR-Takatori accelerogram. In the case of the specimen SC45-25-25H with a value of $T = 0.605$ second for the converted real bridge pier, the relatively large and sudden increase in the displacement occurred at about 5 seconds after the input of the ground acceleration was started (see Figs. 7(a) and 7(b)). At this moment, the nondimensionalized displacement δ/δ_y was as large as 10, and the structure was severely damaged. The subsequent cyclic displacements were still large and difficult to recover from the excessive drift. The natural period T of the real bridge pier converted from the specimen SC45-35-20H is 0.852 second and it is larger than that for the converted bridge pier of the specimen SC45-25-25H. In this case, the induced responses as shown in Figs. 7(c) and 7(d) were smaller than those of the specimen SC45-25-25H. For the third specimen SC45-60-20H, its responses were generally milder. As is seen in Figs. 7(e) and 7(f), the response displacement and dissipated energy were relatively small.

The maximum response displacement (δ_{max}/δ_y) and residual displacement (δ_R/δ_y) of the three specimens are given in Table 3. Plots of δ_{max}/δ_y and δ_R/δ_y against the natural period T are shown in Fig. 8. Thus, it can be found that the responses of structures under earthquake loadings simulated using the JR-Takatori and JMA earthquake accelerograms are very sensitive to the natural period. In other words, these two earthquake accelerograms produce large responses when the structure's natural period is small, for example, $T < 1.0$.

4. Conclusions

Results of the pseudodynamic tests showed that the residual displacement of steel bridge pier can be significantly reduced by filling concrete inside, but the improvement of the maximum response displacement can not be expected. On the other hand, it is found that the natural period of the bridge piers has a large influence on the seismic responses.
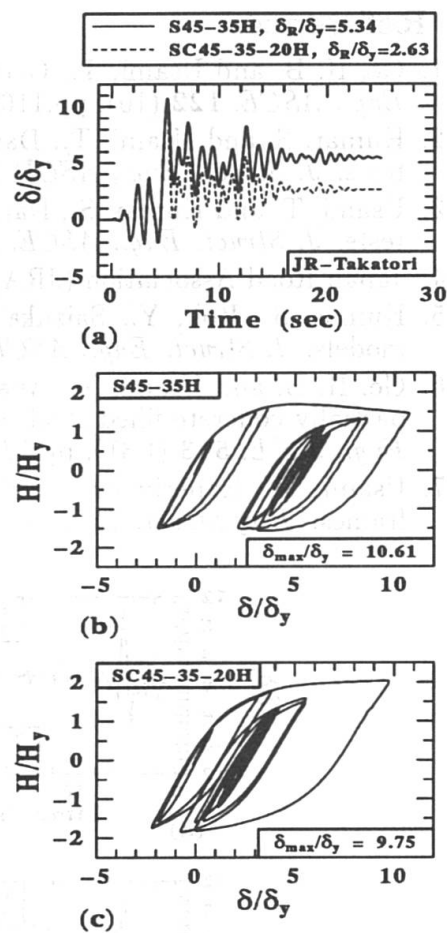

Fig. 5 Effect of h_c/h on Seismic Responses
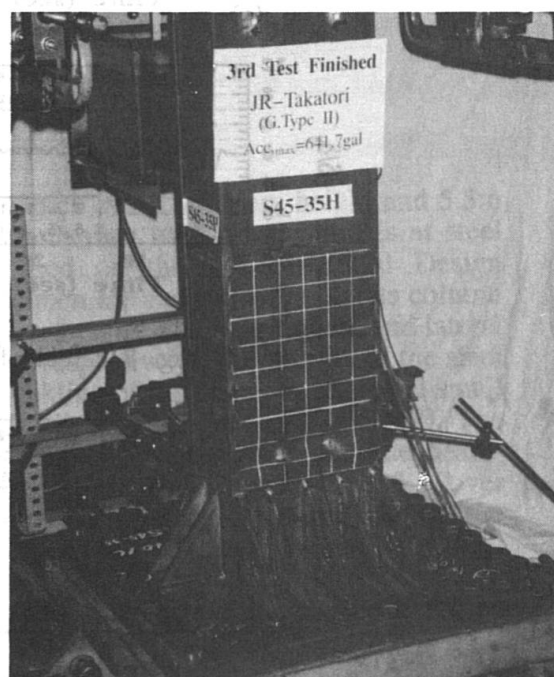
Fig. 6 Damaged Steel Column (*without concrete*)

5. References

1. Ge, H. B. and Usami, T., Cyclic tests of concrete-filled steel box columns. *J. Struct. Eng., ASCE*, **122** (10), pp.1169-1177, 1996.

2. Kumar, S. and Usami, T., Damage evaluation in steel box columns by cyclic loading tests. *J. Struct. Eng., ASCE*, **122** (6), pp.626-634, 1996.

3. Usami, T. and Kumar, S., Damage evaluation in steel box columns by pseudodynamic tests. *J. Struct. Eng., ASCE*, **122** (6), pp.635-642, 1996.

4. Japan Road Association (JRA), *Specification for highway bridges*, 1990 (in Japanese).

5. Kumar, S., Itoh, Y., Saizuka, K. and Usami, T., Pseudodynamic testing of scaled models. *J. Struct. Eng., ASCE*, **123** (4), 1997 (to appear).

6. Ge, H. B. and Usami, T., Analytical study on Ultimate strength and deformation of partially concrete-filled steel beam-columns of box sections. *Struct. Eng./Earthquake Eng., JSCE*, **513** (I-31), pp.77-88, 1995.

7. Usami, T., Experimental verification of ultimate strength formulas for plane rigid frames. *J. of Struct. Eng., JSCE*, **36A** pp.79-88, 1990.

Fig. 7 Effect of T on Seismic Responses

Fig. 8 Effect of T on δ_R/δ_y and δ_{max}/δ_y

Seismic Performance of a Composite Frame Structure

Toshihiko YAMAMOTO
Professor of Civil Eng.
Daido Inst. of Technology
Nagoya, Aichi, Japan

Takeshi OHTAKI
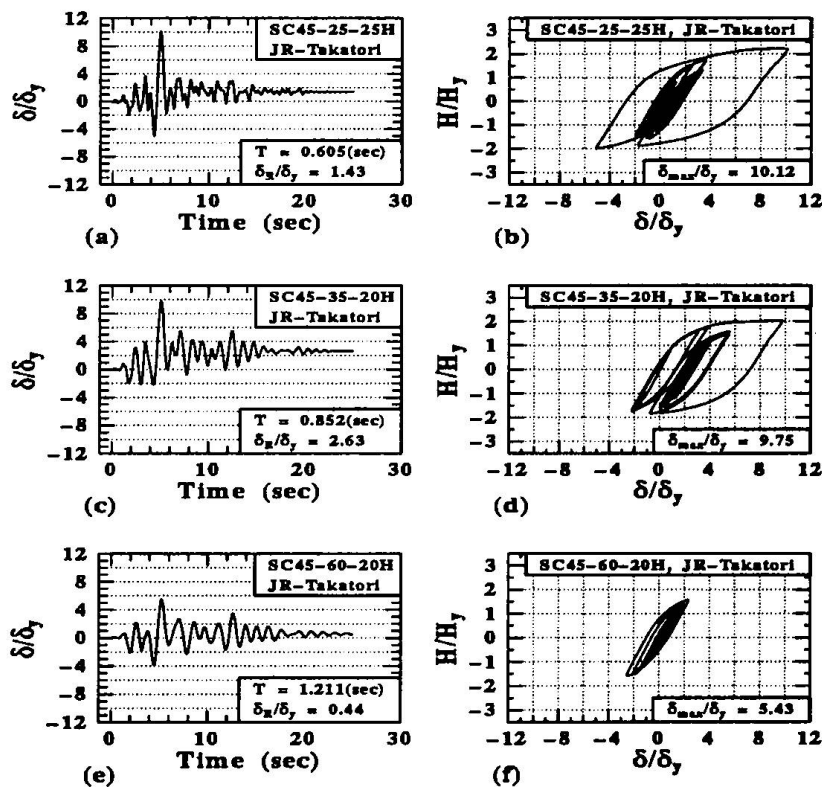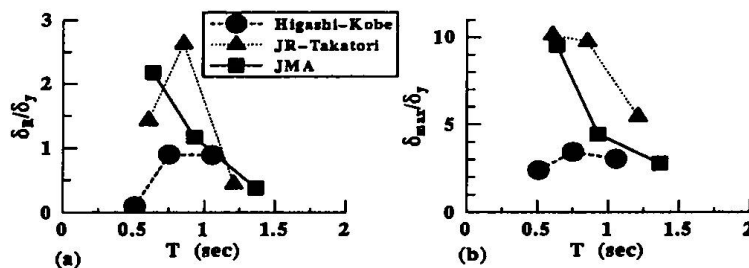Researcher of Civil Eng.
Inst. of Tokyo Construction
Sagamihara, Kanagawa, Japan

Toshihiko Yamamoto, born 1947,
received his doctor degree from Nagoya
University 1989. He is a member of AIJ
Committee, Composite Structure.

Takeshi Ohtaki, born 1961, received his
MEng from Kyoto University 1986. He
has worked on structural dynamics.

Summary

In order to investigate the elasto-plastic behavior of composite frame structure consisting of steel beams and reinforced concrete columns, a full-scale three story and two bay (2.8m story height and 5.5m beam span) frame was tested under cyclic lateral loading. The response of the structure was quite ductile and reached its mechanism with plastic hinges at the beam ends and the first story column bases. No serious damage in beam-column joints except some outer beam-column joints were observed throughout the test.

1. Introduction

The composite frame structure consisting of steel beams and reinforced concrete columns is a structural system which utilizes steel and concrete materials effectively and expected to bear the needs for saving cost and labor for construction. In spite of the advantage, it is important to know the seismic performance of this type of structure when built in seismic zones. In order to demonstrate the elasto-plastic behavior of the composite frame structure, a full-scale three story two bay (2.8m story height and 5.5m beam span) specimen was tested.

2. Experimental Program

2.1 Specimen

Fig.1 shows the full-scale three story two bay specimen which has 2.8m story height and 5.5m beam span. The specimen was designed to provide a mechanism with plastic hinges at steel beams and reinforced concrete first story columns based on the AIJ Structural Design Guidelines[1]. The column and beam sections of the specimen are shown in Fig.2. The column had a cross section of 550mm x 550mm and a 2300mm clear height. The longitudinal and lateral reinforcement ratios of the column were 2.54% and 0.92%, respectively. The section of the steel beam was BH400x150x9x12. In order to prevent lateral buckling of the beam, three lateral small beams were implemented based on the Ultimate Structural Design for Steel Buildings[2]. The thickness of the slabs was 100mm and connected to the beams with stud bolts. The beam-column joints were designed based on the previous test results[3] as shown in Fig.3. Cover plates with shear cotter were used to provide enough bond between concrete and steel in the joints[3].

The mechanical properties of the concrete and steel are shown in Table 1 and 2. The specified concrete strength was 21MPa.
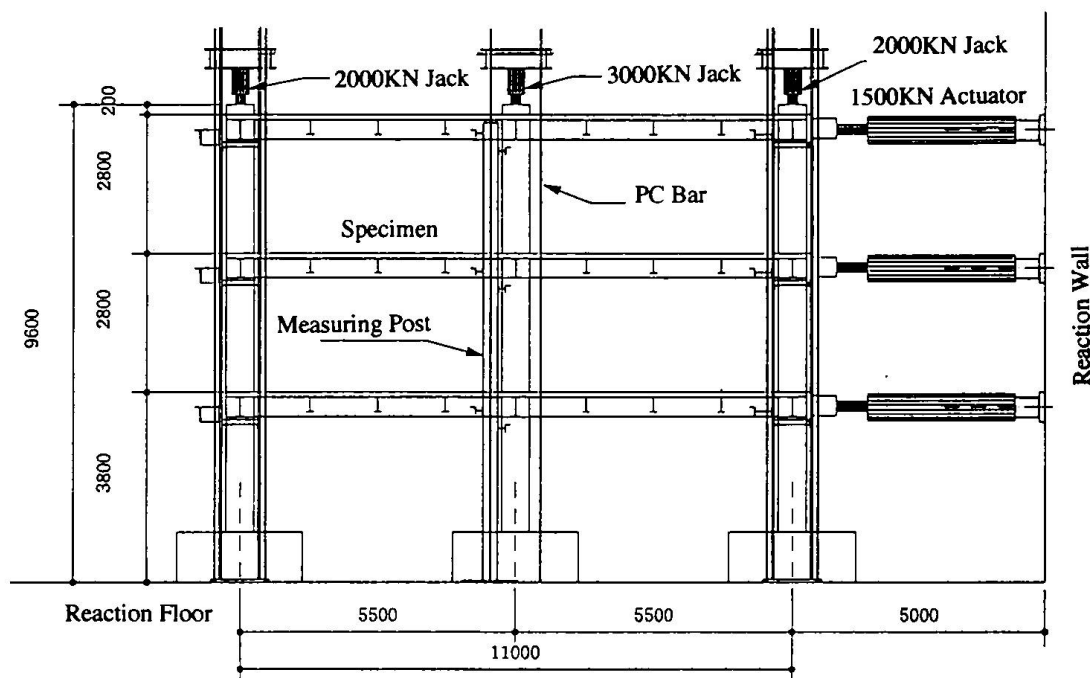
Fig.1 Specimen

Fig.2 Column and Beam Section

Column 12-D29
4-D13 @100

Composite Beam
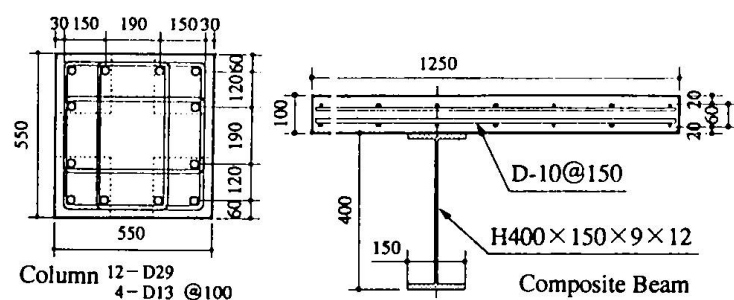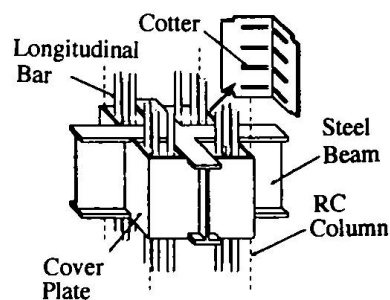
Fig.3 Joint Details

2.2 Test Procedures and Measurements

Prior to the cyclic loading test the natural frequencies, stiffness matrix and flexibility matrix of the frame were measured to examine the elastic behaviors of the structure. The cyclic loading test under inverted triangle load distribution was conducted subsequently. The axial load applied to the top of the inner column was 1600KN and the axial force ratio was 0.25. The load applied to the outer columns was 1270KN and the ratio was 0.20. The lateral shear load was applied to

Position	Fc [MPa]	Ft [MPa]	Ec [GPa]
1FColumn,2FSlab	32.5	2.75	28.1
2FColumn,3FSlab	34.9	2.75	28.3
3FColumn,RFSlab	34.4	2.92	28.9

Fc,Ft:Compressive, Tensile Strength
Ec:Young's Modulus

Table 1 Properties of Concrete

Position	Fy [MPa]	Ft [MPa]	Es [GPa]
Steel Beam Flange	285	441	210
Column Long. Bar	400	577	197
Column Hoop	319	493	177
Slab bar	376	520	191

Fy,Ft:Compressive, Tensile Strength Es:Young's Modulus

Table 2 Properties of Steel

the each floor level with three actuators. The load distribution through three floors was maintained inverted triangular shape from maximum load at RF to zero at base floor. The cyclic loading sequence applied to the specimen was a displacement control defined as the relative deformation angles(R) between base floor and RF, single cycle at 1/1000 and two cycles at 1/400, 1/200, 1/100, 1/50 before reaching ultimate strength.

3. EXPERIMENTAL RESULTS

3.1 Natural Frequencies and Stiffness and Flexibility Matrices

Measured natural frequency of the first mode under non axial force condition was 5.7Hz. The calculated first mode natural frequency obtained from the stiffness and flexibility matrices was about 5.9Hz which gave a good agreement with the directly measured natural frequency.

3.2 Elasto-Plastic behavior

The test results are summarized in Table 3 and the crack pattern at the final loading stage is shown in Fig.4. First flexural cracks were observed in slabs during loading stages of R=1/1000 and 1/800 started from 2F, 3F to RF and propagated rapidly in the following loading stages. Flexural cracking occurred at R=1/600 and R=1/300 in the first story columns and 2nd-3rd story columns, respectively.

Sequence of plastic hinges are shown in Fig.5. The plastic hinge formation was defined as the yielding of column reinforcing bars or beams or slab reinforcing bars. The cracking load agreed well with the prediction. The second floor steel beams yielded at compression side at R=1/240 and the other floor beams except RF beams yielded at compression or tension side between R=1/200 and 1/100. Finally the RF beams and the first floor columns yielded between R=1/100 and 1/75 and formed a total yield mechanism categorized by beam-yield type. After the formation of the mechanism, local buckling was observed in the 2nd and 3rd floor beams at R=-1/60. However beam-column joints did not collapsed.

3.3 Force-Displacement Relationship

Force-displecement relationships are shown in Fig.6. The frame response showed no strength degradation due to cyclic loading at the same displacement angles. Although the hysteresis loops exhibited slightly pinched shape until R=1/100, they showed quite hysterical energy absorption at R=1/50.

The lateral force at the mechanism agreed well with the calculated strength using virtual work method. The relative story drifts at 3rd, 2nd and 1st story were 35.5mm(R=1/79), 45.0mm(R=1/62) and 31.5mm(R=1/89), respectively. The responses of each story of the specimen showed ductile behavior even after the mechanism formed and the frame capacity did not decrease until R=1/25.

The skeleton curves obtained by the elasto-plastic analysis is also shown in the figures with dotted line. In the analysis, the end spring member model considering rigid zone was used. The column and beam were modeled to have tri-linear characteristics as presented in Table 4. The

Displacement Angle R	Remarks	Story Shear[KN]						Story Drift[mm]					
		RF		3F		2F		RF		3F		2F	
		Exp.	Cal.	Exp.	Cal.	Exp.	Cal.	Exp.	Cal.	Exp.	Cal.	Exp.	Cal.
1/1000	Slab Cracking	104	-	166	-	195	-	2.8	-	3.5	-	2.1	-
1/600	Column Cracking	158	148	254	246	300	292	4.9	3.3	5.7	3.8	3.4	2.1
1/240	Beam Yielding	314	355	519	587	616	698	11.4	8.6	13.6	10.9	8.9	7.9
1/75	Mechanism	638	718	1059	1186	1255	1412	35.5	43.8	45.0	59.4	31.5	50.1

Table 3 Results of Test

Fig.4 Observed Crack Patterns
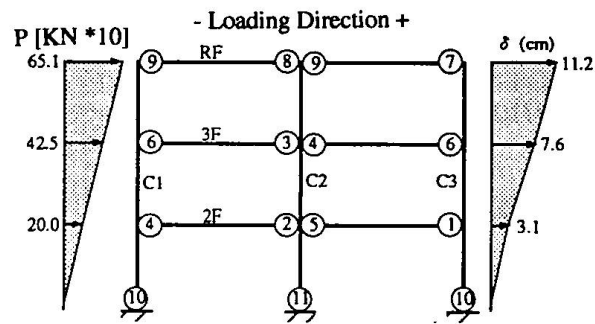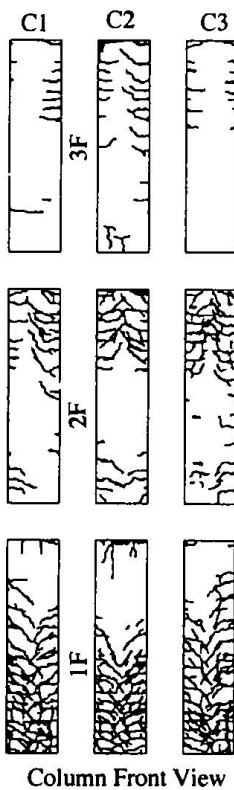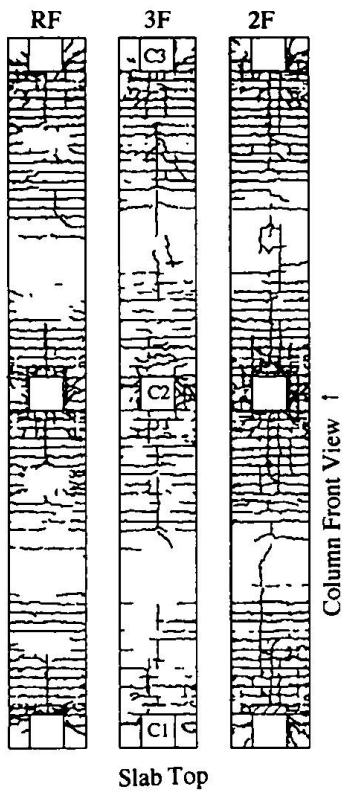
Fig.5 Sequence of Plastic Hinge Formation

Fig.6 Relationships between Story Shear and Story Drift

Column	Inner	Outer	
Cracking Moment [KN m]	225	253	
Yielding Moment [KN m]	841	903	
Effective Moment of Inertia [cm4]	Ie		
	925000		

Composite Steel Beam	Positive Bending	Negative Bending	
Full Plastic Moment [KN M]	Mp	Mp'	
	543	400	
Effective Moment of Inertia [cm4]	cIn	cIn'	
	50100	24300	

Table 4 Model for Column and Beam

of the analysis gave good agreements with the measured lateral force and story drift at the mechanism, with the measured initial and post cracking stiffness.

The equivalent damping factors at each loading stages are shown in Fig.7. They were 2-6% during R=1/1000 and 1/200 and increased to 4-8% at R=1/100. After the mechanism formation, the loop area increased significantly and the equivalent damping factor increased up to 16-19%.

Fig. 7 Equivalent Damping Factor

3.4 Strain Distribution

Fig.8 Distribution of Strain

The strain distribution of the longitudinal rebars of the columns and the steel beams are shown in Fig.8. Large strains were recorded at the first story column base and the strain profiles at the second story column was that of double bending. Although the strains of the third story column rebars were large at the column top, reinforcing bars were well an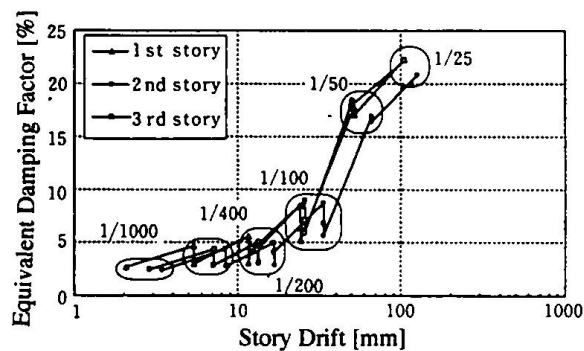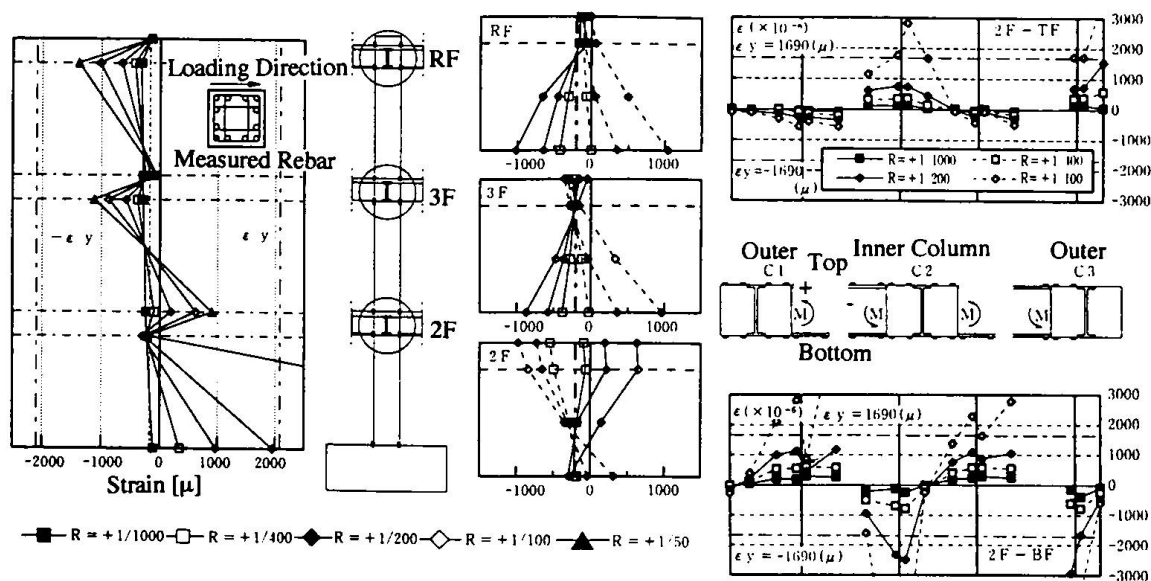chored in the joint at the end of the test. The strain distributions of outer column reinforcing bars were almost the same as that of inner column. The longitudinal bars in the first story columns yielded at the column base at about R=1/75 and the third story column rebars yielded at the column top at about R=1/50.

The observed beam strains at the interior column faces changed from tension-to-compression in the beam-column joint, indicating the stresses were transferred effectively through the joints.

3.5 Joint Behavior

Final crack patterns inside the joint were investigated after the test by cutting off the cover plates. The joints were not heavily damaged and their crack patterns were corresponding to the direction of the shear force transferred through the joints. It is considered that the cover plates with shear cotter were great effective for enhancing the beam column connection.

4. Conclusions

The following conclusions are derived from the test results.
1) The frequencies obtained from the three different measuring technique; direct measurement, stiffness and flexibility matrices, agreed well each other. It is recommended to use flexibility matrix measuring technique for estimating the frequencies of structures because of their relative simplicity.
2) The specimen formed an estimated total yield mechanism of beam-yield type at R=1/75. The response of the specimen showed stable hysteresis loops and excellent ductility. Although the shear capacity was almost the same as that calculated from virtual work method, the deformation was larger than that expected.
3) The elastio-plastic analysis based on measured material strength made an accurate estimates of the test results especially in terms of the occurrence of the cracking.
4) From the strain distribution adjacent the joints, shear force was considered to be transferred well through the joints. Serious damage was not found in the joints.
5) Although it is shown that this type of structural system has an excellent seismic capacity, it is important to control relatively large story drift of the structure, could be a matter for further research.

Acknowledgement

References

[1] Architectural Institute of Japan, "AIJ Structural Design Guidelines for Reinforced Concrete Buildings,", 1994.
[2] Architectural Institute of Japan, "AIJ Ultimate Structural Design for Steel Buildings,", 1975.
[3] Ozawa, J., et al., "Composite Frame Structures Composed of Steel Beams and Reinforced Concrete Columns," Annual Meeting of AIJ, Structural Part C, No.21862, pp.1897-1899, 1992.8.

Ultimate Strength of Composite Structures Using Superposed Strength Method

Bunzo TSUJI
Professor
Kyoto University
Kyoto 606, Japan

Bunzo Tsuji, born 1940, received his doctorate degree from Kyoto University. His main research interests include the constitutive equations of steel and concrete, stability of steel structures, and ultimate strength of steel and composite structures.

Summary

A method to obtain the ultimate strength and the collapse mechanism of composite frames, using the generalized superposed strength method which combines the yield and bond slip conditions of the steel and concrete with the associated flow rule. The collapse load and the collapse mechanism, considering the axial and rotational deformations at the plastic hinges and the bond slip deformation at the column base, differ from those estimated by the simple plastic analysis. The diaphragm effect of the concrete slabs changes the collapse mode from overall to local side sway mechanism.

1. Introduction

In the design of composite structures in Japan, the superposed strength method has been employed. The author already presented a method to obtain the generalized superposed strength by combining the yield condition of composite members with the associated flow rule, and showed that the method can be applied in the case when the bond between a concrete and a steel is lost and slip deformation occurs.[1.2] This paper presents a method to obtain the ultimate strength of the composite frames under the vertical and horizontal forces considering the yield and slip conditions of the composite members, and to obtain the collapse mechanism considering the plastic and slip deformations derived from the associated flow rule.

2. Ultimate Strength of Composite Members

Fig.1 shows a composite member having a rectangular cross section with an ideal I-section steel. The cross section is idealized into three points model such as shown in the figure. If the stress vs. strain relationship is assumed to be rigid-perfectly plastic for both concrete and steel, such as shown in Fig.2, the yield condition of the steel is a diamond shape and the condition of the concrete is a hexagonal shape, under the axial force and bending moment, such as shown in the Fig.3 (a). The associated flow rule shows that the ratio between the axial elongation e and the rotation ω (Fig.3(c)) is constant on each ridge line of the yield surface such as shown in the Fig.3(b). By summing the strengths of the two materials so that the deformation increments of the elements coincide, the generalized superposed strength can be obtained. According to the flow rule, plastic deformation increment can be given as

$$e = -(D/3)\omega \qquad for \quad -_s N_o \le N \le_c N_o/3 \tag{1a}$$

$$e = 0 \qquad for \quad _c N_o/3 \le N \le 2_c N_o/3 \tag{1b}$$

$$e = (D/3)\omega \qquad for \quad 2_c N_o/3 \le N \le_c N_o +_s N_o \tag{1c}$$

where $_sN_o = 2_s\sigma_o A_f$ and $_cN_o = _c\,\sigma_o\,BD$.

If the anchorage of the steel member is not perfect, slip deformation between the steel and

	Steel	Concrete
	Af	DB/3
		DB/3
	Af	DB/3

3 Points Model
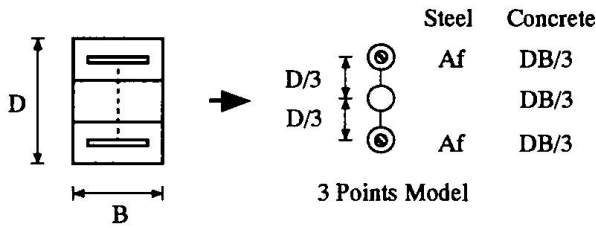
Fig.1 Model of composite cross section
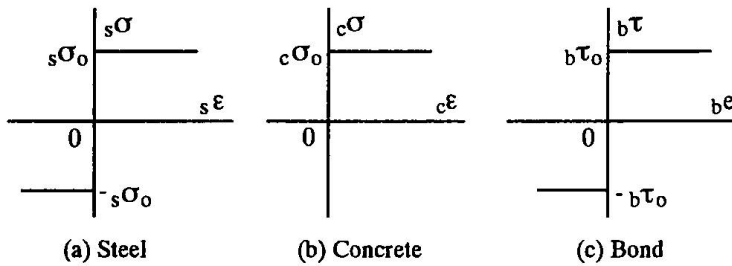
Fig.2 Stress-strain and bond stress-slip displacement relations

(a) Steel (b) Concrete (c) Bond

(a) Yield Condition (b) Flow Rule (c) Plastic Hinge

ω :rotation
e :elongation

$\tan\alpha = e/\omega$
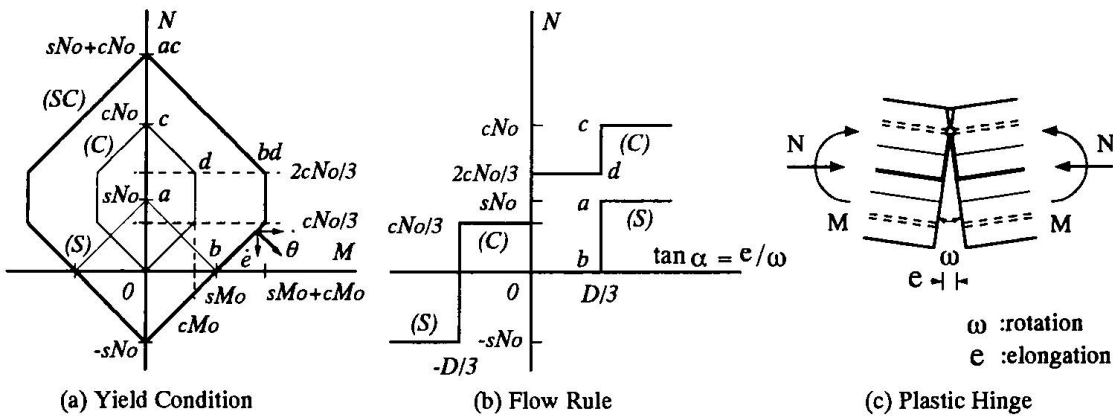
Fig.3 Yield condition and associated flow rule

(a) Yield and Slip Conditions (b) Plastic and Slip Deformations

$_be$: slip deformation
e : axial deformation
ω : rotation

Fig.4 Yield and slip conditions and deformation mode

concrete can occur. Using the bond stress vs. slip deformation relation shown in Fig.2(c), the yield and slip conditions considering the bond slip is obtained such as shown in Fig.4. The bond strength of the steel $_s N_b$ can be given as

$$_s N_b = _b \tau_b l_b S \tag{2}$$

where $_b l$ is a development length of the steel and $_b S$ he circumferential length of the steel cross section. At the stress state shown as the vector $\underline{OA}$, both plastic and slip deformations can occur. Fig.4(b) shows a deformation mode of a column base when both plastic (ω,e) and slip deformations ($_b e$) occur.

3. Ultimate Strength and Collapse Mode of Composite Structures

3.1 Design of Composite Frames

The composite frames subjected to the vertical loads and the lateral forces are designed to collapse by forming the plastic hinges at the beam ends and the column bases (overall collapse mechan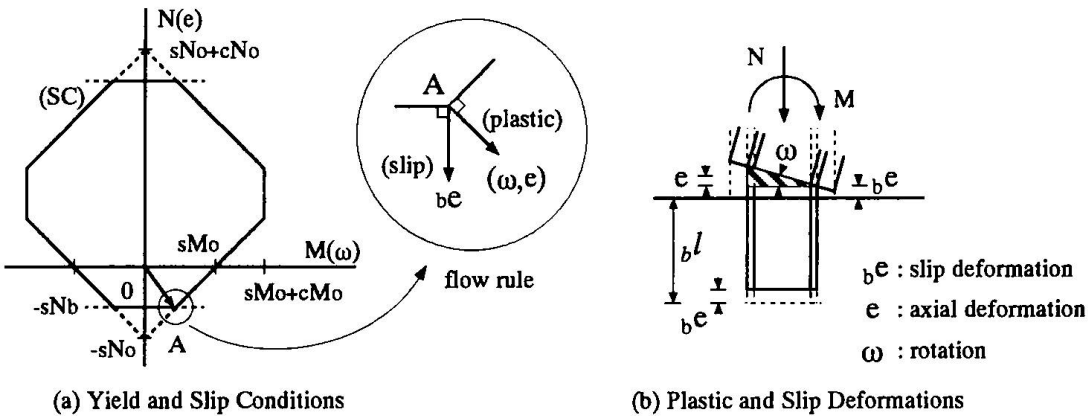ism), using the simple plastic analysis. Lateral loads are specified in conformance with the Building Standard Law of Japan, assuming that the base shear coefficient is equal to 0.3. For the sake of simplicity, we assume that the cross sections of the beams are the same ($D_b/2 \times D_b$) and the cross sections of the columns are also the same ($D_c \times D_c$), such as shown in Fig.5. The magnitude of the plastic moment of each member is adjusted by the cross sectional area of the formed steel.
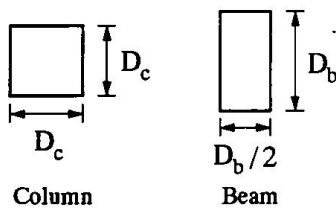
Fig.5 Beam and column cross section

3.2 Portal Frame

A portal frame under the vertical load W and the lateral load 0.3W is shown in Fig.6(a), and the location of plastic hinges obtained by the simple plastic analysis and the plastic moment of each member are shown in Fig.6(b). As the axial load levels of the columns and beams are low, the axial elongation and the rotation are supposed to occur at each plastic hinge. The collapse mechanism of the frame is shown in Fig.7(a). In the parentheses, the rotation angles of the plastic hinges are shown. The equation of virtual work is given as

$$\alpha 0.3 Wh(\omega_1 + \omega_2) - W(\omega_1 + \omega_2)(D_c / 3) \tag{3}$$
$$= 0.18 Wh(\omega_1 + \omega_2) + 0.12 Wh(\omega_1 + \omega_2 + 2\omega_3)$$

where α show the collapse load factor. Assuming that the aspect ratios of the columns (D_c / h) and a beam (D_b / l) are equal to 10, the collapse load factor is calculated as

$$\alpha = 1.1120 \tag{4}$$

Fig.6 Portal frame

The relations between the rotation angle of the members are given as

$$\omega_1 = [1 - 2(D_b / 3h)/ K_1]\omega_2 \tag{5a}$$

$$\omega_3 = (D_c / 3l)(\omega_3 - \omega_1) \tag{5b}$$

where $K_1 = 1 + (D_b / 3h)\{1 - (2D_c / 3l)\}$.

Equation (5a) shows that the rotation angle ω_1 is smaller than ω_2, due to the elongation at the plastic hinges of the beam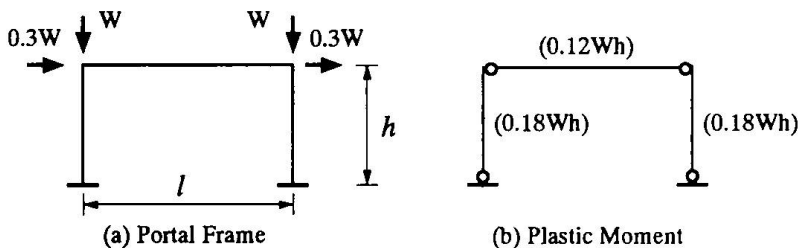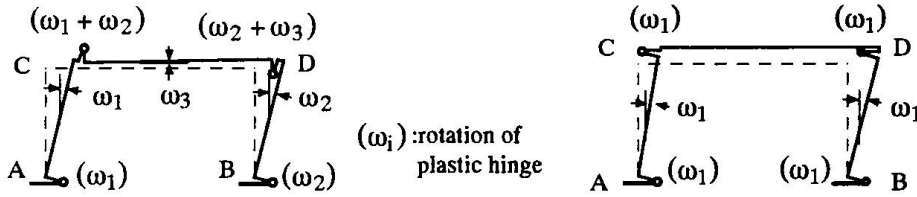. The composite frames usually have a concrete slab. If the diaphragm effect of the concrete slab is perfect, the elongation of the beam is prevented. The collapse mechanism in this case is shown in Fig.7(b). The plastic hinges are formed at both ends of the columns. The collapse load factor is calculated as

$$\alpha = 1.4667 \tag{6}$$

(a) Collapse Mechanism without Slab Diaphragm Effect   (b) Collapse Mechanism with Slab Diaphragm Effect

Fig.7 Collapse mechanisms of portal frame

3.3 Multi-story Frame

Fig.8(a) shows a three-story frame under the vertical and horizontal loads. According to the simple plastic analysis, the plastic hinges are formed at the beam ends and the column bases. Considering the elongation as well as the rotation at the plastic hinges, the collapse mechanism, such as shown in Fig.8(b), can be obtained . In this case, the additional plastic hinges are formed at the lower end of the left columns. The collapse load factor is calculated as

$$\alpha = 1.0522 \tag{7}$$

The relations between the rotation angle of the columns are given as

$$\omega_1 = [1 - 2(D_b / 3h)/ K_1]\omega_4 \tag{8a}$$

$$\omega_2 = [1 - 2(D_b / 3h)^2\{1 - (2D_c / 3l)\}/ K_1^2]\omega_4 \tag{8b}$$

$$\omega_3 = [1 - 2(D_b / 3h)^3(1 - (2D_c / 3l))^2 / K_1^3]\omega_4 \tag{8c}$$

where $K_1 = 1 + (D_b / 3h)\{1 - (2D_c / 3l)\}$.

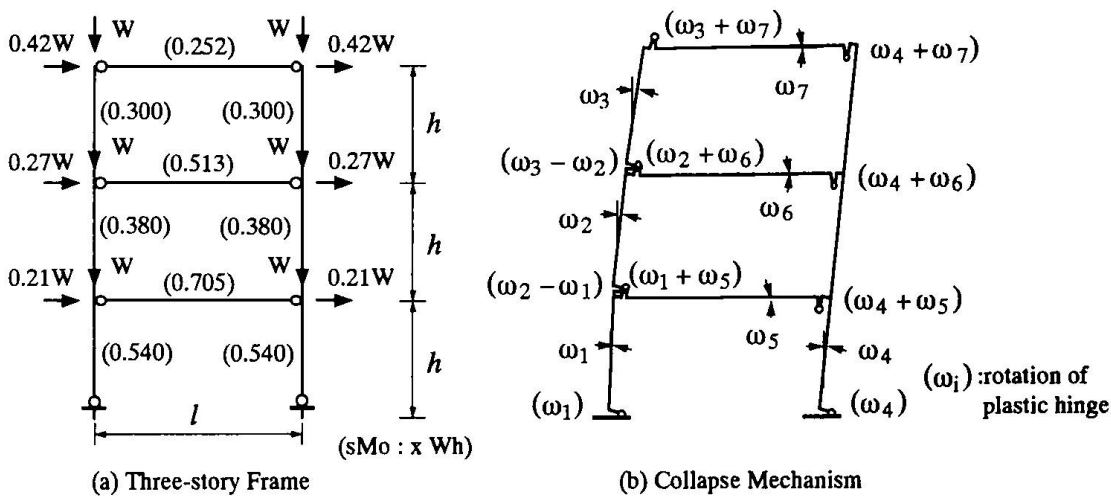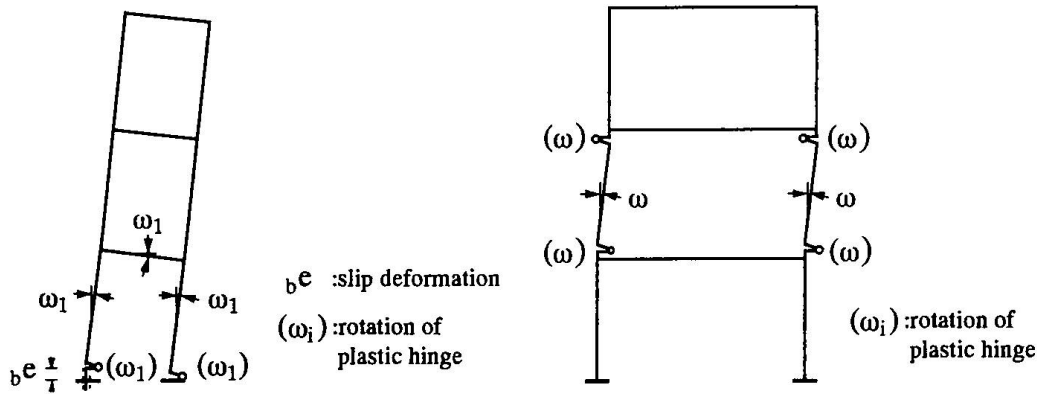(a) Three-story Frame   (b) Collapse Mechanism

Fig.8 Three-story frame and the collapse mechanism

(a) Collapse Mechanism Considering Slip Deformation   (b) Collapse Mechanism with Slab Diaphragm Effect

Fig.9 Collapse mechanisms of three-story frame

The difference between the rotation angle of the left and right columns decreases in geometric progression as the number of storys increases, showing that the deformation of the plastic hinges at the lower end of the left columns decreases as the story number increases.

In the case of a slender frame whose beam span (l) to column height (h) ratio is equal to 0.5, tension force acts at the left column base. If the anchorage of the steel is not perfect, the slip deformation as well as the plastic deformation may occurs at the column base. The collapse mechanism in this case is shown in Fig.9(a). The plastic hinges are formed only at the column bases, and the sip deformation is observed at the left column base. The collapse load factor in this case is calculated as

$$\alpha = 0.9938 \tag{9}$$

when the bond strength of the steel at the column base is given as $_sN_b = 0.15\,_sN_o$. The result shows that collapse load is smaller than the load obtained using the simple plastic analysis. Consider again the frame shown in Fig.8(a). If the diaphragm effect of the concrete slab is perfect, the elongation of the beams is prevented. The flow rule shows that the bending strength of the beams increases up to $_sM_o +_c M_o$, when only the rotational deformation is permitted, as shown in Fig.3. The collapse mechanism in this case is shown in Fig.9(b). Only the side sway mechanism of the second story occurs. The collapse load factor is calculated as

$$\alpha = 1.1981 \tag{10}$$

3.4 Multi-bay Frame

Fig.10 shows a one story multi-bay frame. According to the simple plastic analysis, plastic hinges are formed at the beam ends and the lower end of the columns. Considering the elongation and rotation of the plastic hinges, the collapse mechanism such as shown in Fig.11 can be obtained . The rotation angle of the m-th column can be obtained as

$$\omega_m = \{1 + (2D_b /3h)/ K_3\}^{m-1}\omega_1 \tag{11}$$
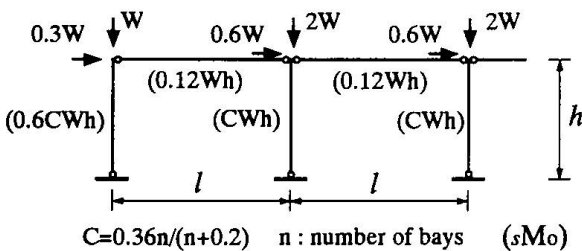

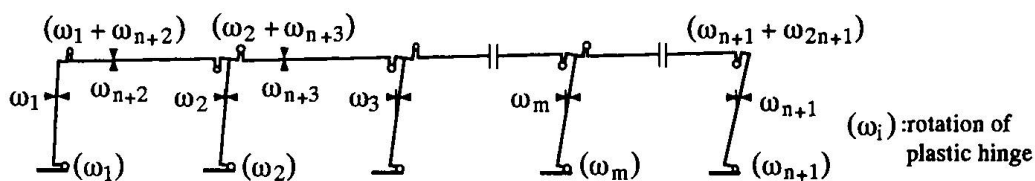C=0.36n/(n+0.2)   n : number of bays   ($_sM_o$)

Fig.10 One-story n-bay frame

Fig.11 Collapse mechanism of n-bay frame

where $K_3 = 1 - (D_b/3h)\{1 + (2D_c/3l)\}$.

The rotation angle of the column increases in geometric progression as the number of bays increases, due to the elongation of the beams. Assuming that $l/D_b = 10$ and $h/D_c = 10$, the relation between the rotation angle ω_1 and ω_n is obtained as

$$\omega_n = 1.14354^{n-1}\omega_1 \tag{12}$$

When the number of bays is n=6, Equation(12) gives $\omega_n = 1.9955\omega_1$, showing that the rotation angle of the right side column is twice of the left side column.

4. Conclusions

This paper presented a study for obtaining the strength and collapse mechanism of the composite frames, considering the axial and rotational deformations at the plastic hinges. Major findings obtained from this study are as follows:

(1) The collapse load and collapse mechanism of the composite frames differs from that estimated by the simple plastic analysis, due to the axial and rotational deformations at the plastic hinges. Except for one story frames, additional plastic hinges should be formed at some column ends.

(2) The axial and rotational deformations at the plastic hinges differ from one hinge to another. The relation between the rotational deformations of the plastic hinges at the column ends can be given in geometric progression form, as the number of bays or number of storys increases.

(3) When the diaphragm effect of the concrete slab is perfect, the collapse mode of the composite frames changes from overall side sway mechanism to local (one story) side sway mechanism.

References

[1] Tsuji,B. Wakabayashi,M. and Sugahara,M.: Ultimate strength of composite beam-columns, Proc. of Inter. Conf. on Steel-Concrete Composite Structures, Fukuoka,1991,pp.275-280.

[2] Tsuji,B. and Wakabayashi,M.: Ultimate strength of composite beam-columns and beam -column joints using superposed strength method, Proc. of plasticity'95, 1995, pp.467-470.

Steel-Concrete Seismic Resistant Structure for Multi-Storey Buildings

Valeriu STOIAN
Prof., PhD, Civil Eng.
Politechnica University
Timisoara, Romania

Valeriu Stoian, born 1949, received
his civil engineering degree at the
Politechnica of Timisoara in 1972
and his PhD in 1982. He is Professor
of structural engineering at Politechnica
University of Timisoara and Technical
Manager in a building construction
enterprise, being involved in major
building projects.

Irina OLARIU
Civil Eng.
CADFEM-10 Ltd.
Timisoara, Romania

Irina Olariu, born in 1945, received
her civil engineering degree at the
Politechnica of Timisoara in 1968.
She is structural engineer in a design
office in Timisoara. Her activity is
related to structural analysis,
structural modelling and CAD.

Summary

The building structure was designed to resist seismic action. Therefore specific details were conceived to satisfy anti-seismic provisions according to Romanian seismic codes.
Composite beams were designed as steel beams interconnected with the reinforced precast concrete slabs with shear connectors. Steel concrete composite column has structural steel made up by steel welded bands and reinforcement realised from steel rolled bars.
Special attention was paid to the structural model to perform the linear modal analysis and to obtain the non-linear behaviour of the structure.

1. The building assembly

The construction belongs to a building assembly composed by three main buildings having different number of stories, being separated by an interior street covered with transparent glass. The functional requirement to have wide spaces at each level, led to a skeletal scheme for the buildings. Being placed at the ground level, the interior street floor slab connect only functionally the buildings, thus each of them has an independent behaviour and it was design accordingly to this assumption. Structurally being conceived similarly, the design process was identical for all three buildings.

2. Structural system

The main construction is a multistory building consisting of 9, partially 12 levels (Fig.1).
The underground level consists into an rigid box made up from reinforced concrete realised from an assembly of structural walls together with the floor and footings. The upper levels are realised as space skeleton bar structure using plane frames placed on two orthogonal directions, being connected through the floor slabs (Fig.2).
The entire structure is realised as a steel-concrete composite construction. The structural solution is justified by the span width with unexaggerated cross sectional dimensions for the columns, adequate lateral stiffness and cost effective fire protection due to the presence of the concrete.
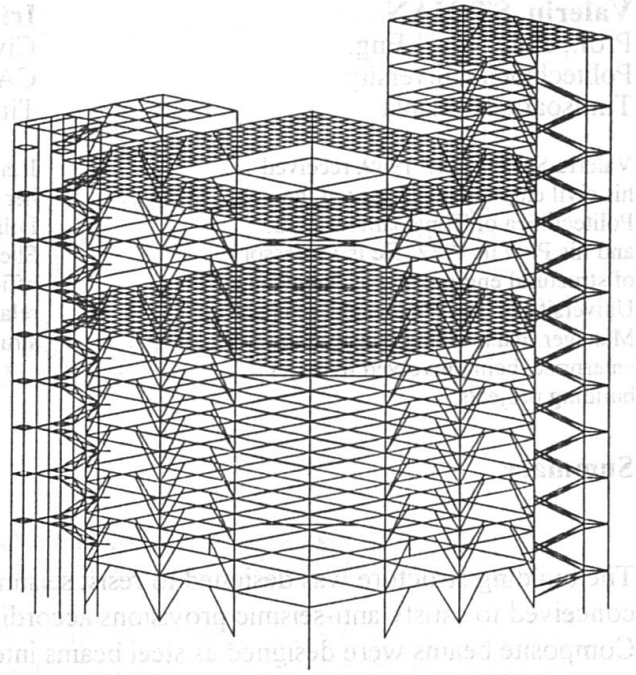
Fig. 1 Front view of the multi-storey building   Fig. 2 The space bar model of the structure

2.1 Structural detailing

The building is placed into an seismic zone (with the ratio between the peak ground acceleration to the acceleration of gravity equal to 0.16). In order to perform the analysis, the cross sectional characteristics of the building elements were considered accordingly with the loading type (long term loads, short term loads).

No infill panels were considered in the structural model. Therefore, a joint between the infill masonry and the structural elements was provided.

The columns have squared section because of the beam spans which are identically on both directions. The main stress state in columns is eccentric compression with bending moments approximately equal on both directions. Load bearing capacity to torsion is neglected due to the existence of the floor slab and due to the minor value of the torsion capacity of the secondary steel beams simply supported on the main beams. All the joints are welded. For the steel elements of the structure were utilised the specific dimensions presented in Tab. 1, in which A is the cross sectional area and U is the perimeter of the cross section.

ELEMENT	Frame beams	Secondary grid beams	Braces
A/U (m)	100-165	160-240	115-160

Tab. 1 A/U ratio for the structural elements

The steel-concrete composite frame beams are **I** sections obtained from welded steel bands connected at the upper flange with the reinforced concrete slab by shear connectors.

The beams were provided with full web at the extremities and with holes in the middle span to access technological ducts. Those without braces were designed at permanent loads, those with braces at seismic loads. The floor slab are realised by precast reinforced concrete slabs monolithically connected at the upper part of the supporting beams. For the inner space between the main beams an rectangular simply supported steel grid was provided. The secondary beams were realised also as composite beams.

The Romanian anti seismic code provisions (P100) imposes for frames rigid connections between beams and columns, the steel beams were designed as follows: two cantilevers welded at the columns adjacent to beam span by the complete penetration technology and a central part which will be welded at yard. An typical detail of the steel joint is represented in Fig. 3. The overall stability in the final phase of the beams was established through the beam connectors which connect the beams with the horizontal diaphragm - the floor slab. The shear connectors are of rigid type and consist of I steel profile welded on the top flange of the beam (Fig. 4).
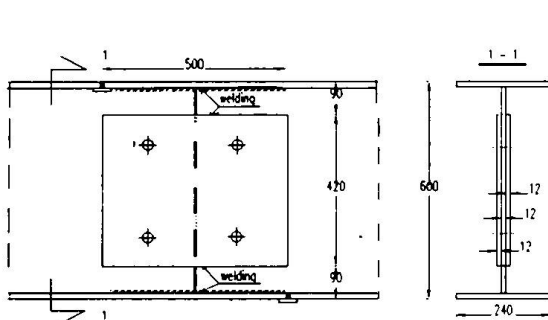

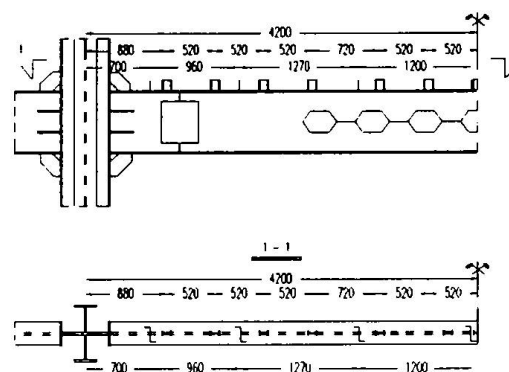
Fig. 3 The typical beam connection   Fig. 4 Beam connectors

Due to alternate stresses in the seismic load, in the seismic beam design, at the ends the contribution of the reinforced concrete slab was neglected. The stability of the inferior part of the cross section near the beam column joint was assured with two pairs of horizontal stiffeners, Fig. 5. In the same time, the condition which impose an higher capable moment in the joint section with 20% than of the beam section ($Mj/Mb > 1.2$) was respected at every joint. The specific detail was conceived taking into consideration the concept, generally recognised now, which located the energy dissipation zones out of the joints. Thus, the special conditions provided in P100-92 for the potential plastic zones at beams were respected. The columns were designed and realised as steel-concrete composite section, using EC4 code (Commission of the European Community, 1992). An typical detail is represented in Fig. 6. The structural analysis revealed that the structure is not sensitive to second order effects.

2.3 Structural stiffening

In order to avoid large lateral displacements of the structure, a set of steel braces are provided, as can be seen schematically in Fig. 2, in which can be seen also the braces positioning. Based on recent conclusions resulting from a large number of theoretical and experimental works it was adopted an eccentrically braced solution. The braces efficiency was evaluated by the relative level stiffness of an unbraced or braced structure and by seismic forces acting on unbraced and braced frames. Two variants of braces positioning were studied:
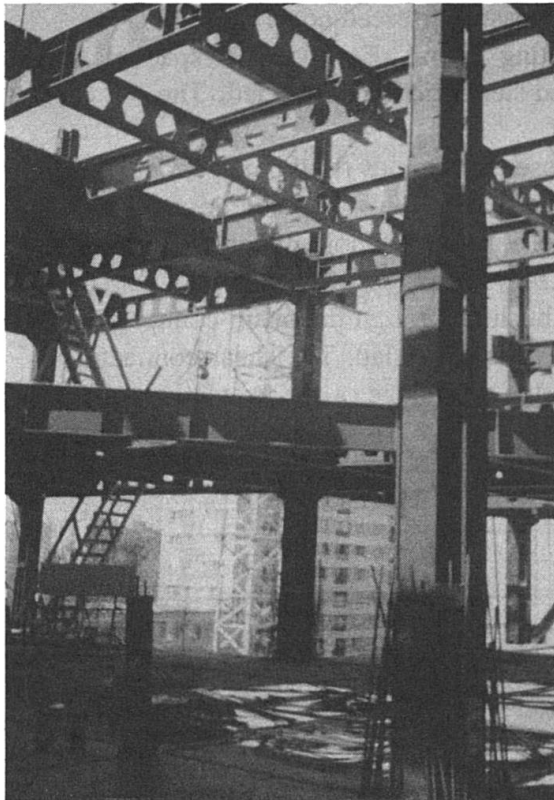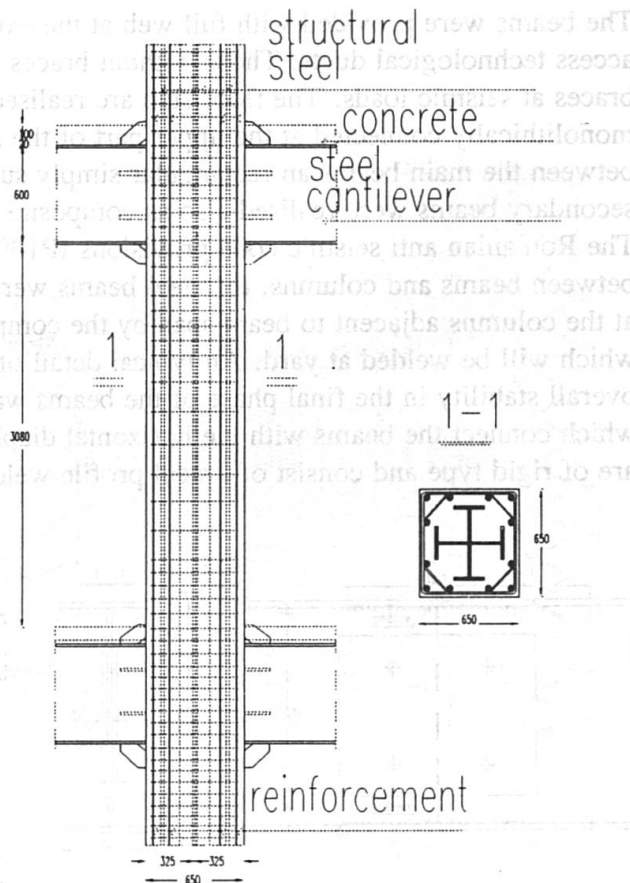
Fig. 5 Structural steel detail   Fig. 6 Composite steel concrete column detail

■ A variant - at which the braces are placed on the exterior part of the building in two consecutive spans on each side.

■ B variant - at which the braces are placed in the four corners of the exterior part of the building

The square form of the horizontal building plane admits as symmetry axes both the sides and the diagonal. These axes will be found in modal analysis as principal axes, thus:
- side, if it will be accentuated the stiffness upon the side (variant A);
- diagonal, if it will be placed corner braces (variant B) and eccentrically mass positioning.
In this situation the dynamic structural response is coupled. Therefore, providing the braces in the central spans (variant A) has advantage in the distribution of the axial forces due to horizontal loads. Variant B give a coupled dynamic response of the structure and determine a higher general torsion moment. Absolute and relative displacements reflect the monotone character of the structure, with different values at the top levels for the two studied cases.
The modal response of the structure, lateral displacements and the relative level stiffness are affected by the number of braces rather than their position.

	T1 (s)	T2 (s)	T3 (s)	T4 (s)	T5 (s)	T6 (s)	d_{max}/H_{level} (mm/m)	d_{min}/H_{level} (mm/m)
VARIANT A	1.48	1.43	1.12	0.55	0.54	0.40	10.356	3.3
VARIANT B	1.53	1.47	1.37	0.55	0.53	0.48	22.372	3.48

Table 2. Structural modal response

As it can be seen in Table 2, the maximum drift (including postelastic displacements) overpasses the maximum allowable drift (7 mm/m) for this type of building in spite of the presence of the steel braces.

2.4 Effect of initial stresses

Erection technology generates initial stresses in the structural steel of the columns. Thus, initial compression stresses in the cross section of the structural steel is about 30 MPa, respectively an initial strain $\varepsilon_i = 0.15$ mm/m. This strain can be represented as a translation in the strain diagram (Fig.7).
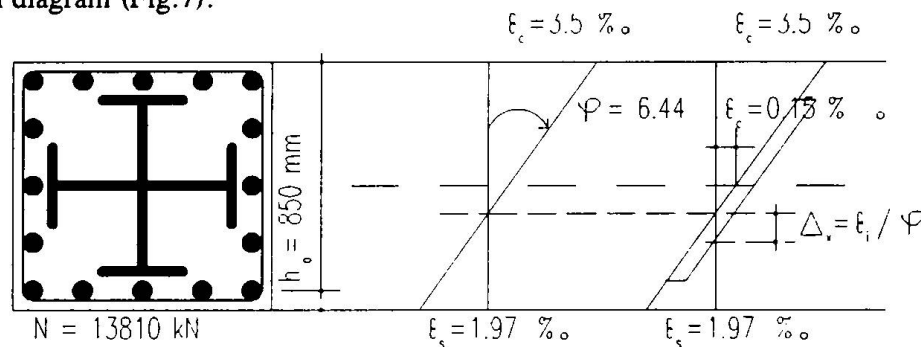

Fig. 7 Influence of the initial stresses

This translation can be quantified with two parameters: rotation φ and axial strain ε_i. Neutral axis will move down with Δ_x, increasing the height of the compression zone. The effect will be the increasing of the sectional ductility together with an reduction of the load bearing capacity of the column.

3. Nonlinear analysis

In order to provide a satisfactory behaviour of the eccentrically braced frame system during the earthquake motions and to determine the collapse scenario of the structure, an non-linear analysis was performed with dedicated software (ANELISE). Was check the collapse mechanism type based on the strength hierarchy. For the nonlinear analysis an condensed model was used. The structural condensed model was subjected to three different accelerograms: Vrancea 1977 (81%), Bucuresti 1986 (100%), El-Centro 1940 (52%). In the Table 3 a short synthesis of the linear and nonlinear structural analysis is presented. In this table, A_{gr} is the ground acceleration, V_{gr} is the ground velocity, E_{ind} is the induced energy and E_{dis} is the dissipated energy, H is the total height of the structure.

CASE	FORCE (kN)	F.POS (H/H_{max})	DISPL (mm)	ROT (rad)	A/A_{gr}	V/V_g	E_{ind} (kNm)	E_{dis} (kNm)
CODE	5149.62	.56	255.6	0.0097				
ACC1	16363.7	.39	302.2	0.0237	3.4	2.07	5083.5	1286.3
ACC2	6185.42	.48	66.2	0.0028	2.4	2.27	520.3	0.0
ACC3	6005.55	.45	77.9	0.0027	2.36	1.77	447.3	0.0

Table 3. Structural response to seismic loads

The collapse mechanism of a braced steel frame with eccentrically placed braces was suggested by the relative ratio between the capable bending moments versus the effective bending moments on the frame beam. The design idea was to avoid the braces stability loose before the beam plasticity. The top level displacements and the required ductility in columns are represented in Fig. 8.
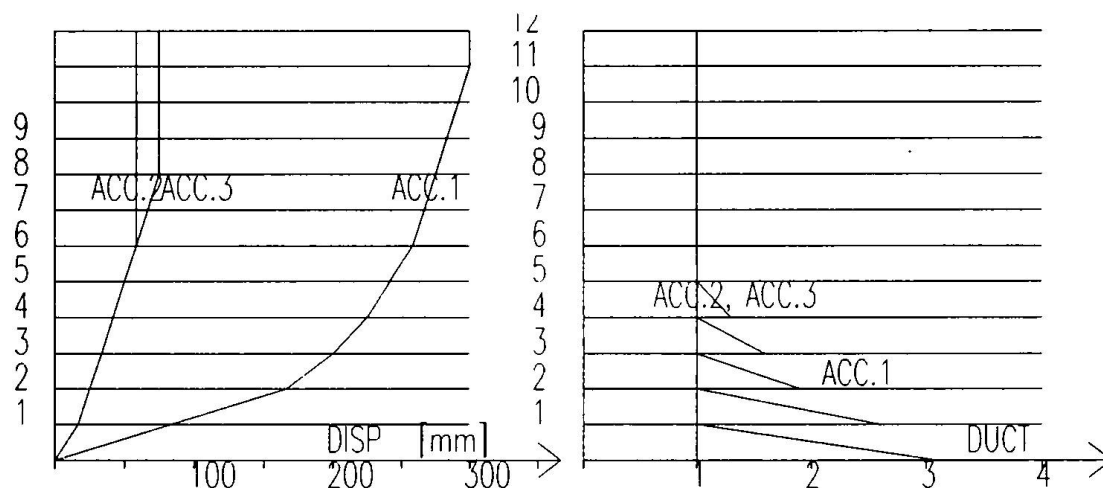

Fig. 8 Lateral displacements and column required ductility

The analysis shows that the structure has an typical frame structural behavior, even in the presence of the braces. The structure is sensitive to Vrancea type accelerograms which has an low incidence in the region where the building is placed. Seismic loads and lateral displacements demonstrate that the reduction coefficient for seismic loads was well choose for the accelerograms 2 and 3. For these accelerograms no plastic hinges were detected and any ductility requirements, the structure remaining in serviceability limit state. For severe earthquakes this structure is mainly governed by a moment braced frame behaviour and the structure goes into the damageability limit state.

The anchorage section for the structural steel of the column was provided at the midheight of the underground level for several reasons such as: incompatible dimensions of the anchorage zone with the column section, avoid to create a shear sensitive section at the base of the structure, inconsistent provisions for the composite steel-concrete column base sections, difficulties for the detailing design in these sections and insufficient knowledge of the behaviour of these anchorage zones.

References

Ministry of Public Works, Romania 1992. P100. Code for the Earthquake Resistant Design of Civil, Industrial and Agricultural Buildings, Bucharest.

Commission of the European Communities, 1992. Eurocode 4. Design of Composite Steel and Concrete Structures.

ANELISE (1993) Time-history analysis of plane frames subjected to static and dynamic loads having elastic and plastic behavior, IPCT Bucuresti.

Dynamic Response of a High-Rise SRC Building Model

Xiangyu GAO
Associate Professor
South China Const. Univ.
Guangzhou, China

Dr. Xiangyu Gao, born in 1959,
received his doctor degree in
Tsinghua University, China.

Fulin ZHOU
Professor
South China Const. Univ.
Guangzhou, China

Fulin Zhou, born in 1939,
received his master degree
in University of Columbia,
Canada.

Xiangsheng XU
Senior Engineer
The Fourth Design & Res. Inst.
Zhuhai, China

Xiangsheng Xu, born in 1961,
received his bachelor degree in
Hefei Industrial University,
China.

Abstract

A 68 story (224m high) S.R.C. high-rise building will be constructed in Guangzhou City, China.
The building has two towers that are connected with over bridges at the 15th floor and the 50th
floor. On the top, there is a ball shaped house (30 meter's diameter) for sightseeing (fig.1).

Shaped steel and reinforced concrete columns (S.R.C. columns) will be used in the building
structure(fig.2). Shear nail, steel brackets welded on the shaped steel are designed in the
columns. These measures are taken to improve the seismic behavior of the building, also to
reduce the section area of columns for increasing usable space.

General structural analysis can not reveal the relative movement between the two towers when
using the hypothesis of rigid floor. The deformations of the thin neck bellow the ball shaped
dining hall may be more serious than the predicted results with normal dynamic models.
In order to verify the dynamic characteristics, to improve the seismic behavior and the reliability
of both S.R.C. members and the connection part between the two towers and the neck, a 1/40
scale steel-concrete model was designed and constructed for shaking table test in the Laboratory
of South China Construction University. White noise random wave and some recorded
earthquake wave were inputted to the 6-DOF shaking table. Accelerations were recorded during
each test.

The testing results and the analysis for the dynamic response of the high-rise S.R.C.model are
introduced in this paper.

General Introduction

Considering the location and the requirements in the anti-seismic design code[1] and structural
design and construction code for high-rise building[2], the designed anti-seismic intensity

of the prototype is 7 degree in Chinese scale. The anti-seismic detail's grade is the first grade[2]. The ratio of length to width of the first plain is 1.9, while the value of slenderness achieves to 4.49. The corresponding values of the core tubes are respectively 1.3 and 12.5. The structure of the neck is '[]' shape S.R.C. shear walls, where the corner shaped steels stretched out from the four columns of the two towers. The floor beams of the dining hall are in S.R.C too, which are welded with shaped steels in the corner columns of the shear walls.
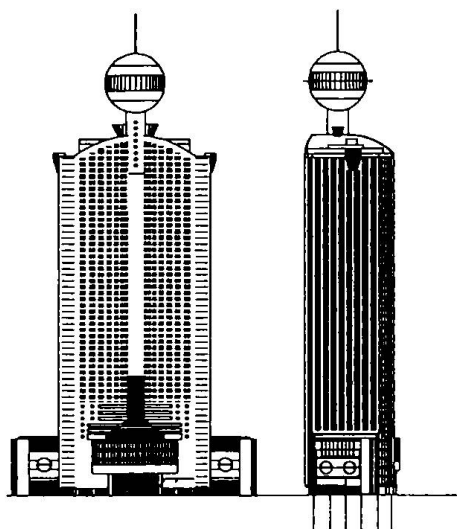
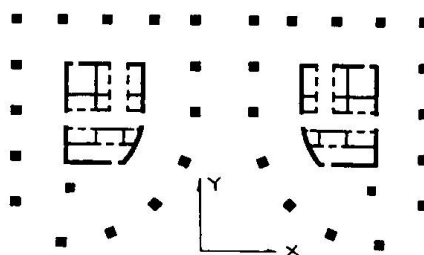*fig.1 Sketch map of the prototype*   *fig.2 S.R.C.colums and R.C. core tubes*

The main objectives of the test research were:
1. To mearure structural frequencies and compare with calculation results.
2. To investigate the dynamic response of the entire structure, including the relative movement between the two towers.
3. To study the reliability of the overbridge and the neck under the ball house.
4. To observe the anti-seismic behavior of the S.R.C. model using the specific details.

Only a small part of the research results is reported here because of the page limitation.

The design and construction of the model

1. The scales of the model
Skirt building was included in the design of the model, because It would affect the seismic response of the main structure. The scale parameters of the model are listed in table 1, according to the similarity theory[3]. The value Ce was determined by considering both the model concrete and model steels, ensuring the equivalence of stiffness contribution to the entire structure.

2. The materials of the model
Concrete was modeled with micro-concrete, because the stress-strain relationship would be similar to concrete. Strength grades of concrete varied from C30 to C60, and the strength of micro-concrete from 6.5MPa to 13.0MPa according to the tests. Model steels were made by fine steel bars. The shaped steels were modeled with thin steel plates(thickness from 0.6mm to 1.0 mm). The mean value of steel module was 196000MPa.

3. The design of S.R.C. column model

If such kind of steel elements were equivalently replaced with model steel rod in elastic model, the post-crack characters and torsion stiffness would be far similar from the original elements in the prototype. From this point, the model shaped steels were made with thin steel plates that were formed and welded as "[]" shape or "I" shape sections. The longitudinal steel bars in beams went through the holes pounced in shaped steels (see figure 3, model S.R.C. columns).

Table 1: Scale Parameter of the Model

ITEM	PARAMETER	SCALE	NOTE
Length	Cl	40	
Area	Ca	1600	
Volume	Cvo	64000	
Elastic modular	Ce	2.60	Considering effective stiffness of S.R.C. element
Stress	Cσ	2.60	
Strain	Cε	1.00	
Density	Cρ	0.40	Considering table weight capacity
Velocity	Cv	2.56	
Accelerate	Ca	0.163	Considering the equivalence of inertia force
Gravity	Cg	1.00	
Frequency	Cf	0.064	
Time	Ct	15.69	
Mass	Cm	25600	
Force	Cforce	4160	
Energy	Cen	166400	

4. The design of model beams

Obviously, the thickness of concrete plate could not be scaled down to model plate (2-4mm) by using micro-concrete, because that it was generally 100-150mm. Ensuring the stiffness contribution of floors to the entire structure similar to the prototype, concrete plate and small beams were modeled with model plates. In this case the bending stiffness could be thought suitable but the shear stiffness might be not.

5. The construction of the model

Some surveying tools were used in the construction of the model for accurate dimensions. Concrete blocks for material testing were ready when the concrete was pouring. Forms were made in bubble plasticity, which could be moved out easily when the model had been finished.
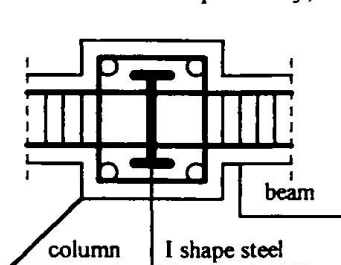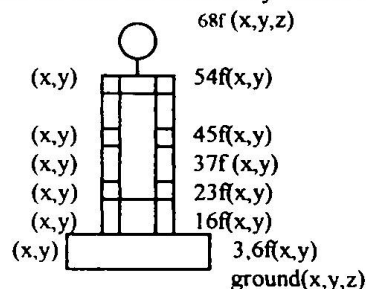

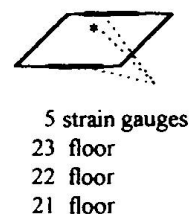fig.3 Model Columns   fig.4 Accelerators arrangement   fig.5 Strain meters

Testing plan

1. The mounting of weights

In order to meeting the requirements of weight similarity and active loads, 4.98 ton weights were needed according to the calculation. The mounting of these weights matched the mass distribution of the prototype.

2. The measuring plan

Figure 4 shows the arrangement of accelerators on some floors. Strain meters were stacked in the place of some connection area (see figure 5). MTS data acquisition system was used for signal recording.

3. The earthquake waves

The Guangzhou wave, Taft wave and El-centro wave were chosen for the test. The lasting time and the amplitude were scaled to fit the needs of the tests. The maximum peak acceleration of each wave was increased from 0.036g, 0.104g, to 0.225g (multiply by C_a)respectively.

4. The testing sequences

Tests began with white noise in each term of intensity. Some tests were arranged in single axis in small and basic intensity, but in the rare intensity test, 2-dimensional earthquake waves were inputted to the earthquake table.

Dynamic behavior of structure

1. Vibration Frequency

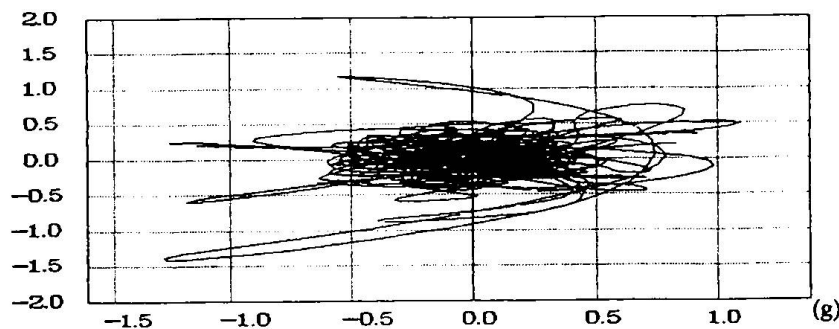Figure 6 gives Taft wave achieved on the seismic table.

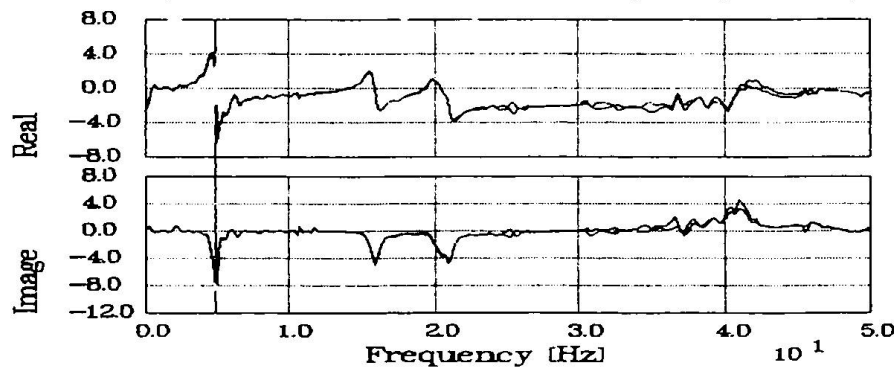fig.6   Taft wave achieved on the table(x and y direction)

fig.7 Transform function (A_{23f} / A_0 in X direction,left tower and right tower)

The fundamental frequency of vibration was 4.88 Hz in x-direction, and 5.07 Hz in y-direction. Figure 7 shows the transform function of acceleration on some floors (A_{if}) to the acceleration input on the table (A_0), by which the frequency points are obvious. Figure 8 gives the vibration mode shapes from data analysis. Table 2 shows the comparison results between the tested frequencies and the calculated results by the program TBSA(mode analysis method, MDF shear model), where the differences come mainly from the rigid floor assumption and the concrete module without considering steel ratio. Table 3 gives corresponding values in the stage of rare intensity, from which frequency decline could be noticed.

Mode1x   · Mode2x   Mode3x   Mode4x
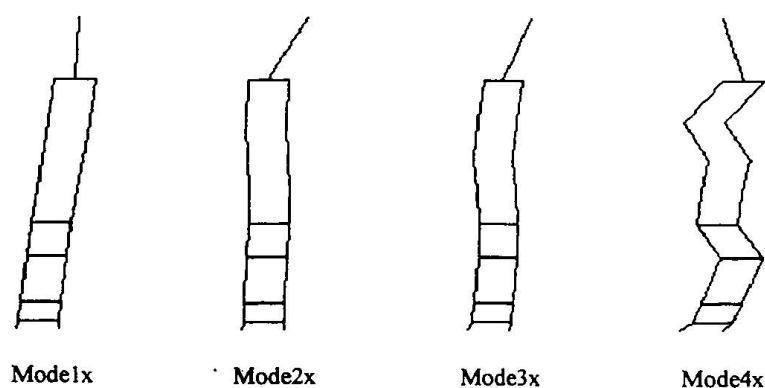
fig.8 Vibration mode shapes tested(X-Direction)

2. Peak acceleration and displacement distribution

Fig.9 and fig.10 give the lateral acceleration and displacement distribution along the height of the model. Considerable relative movement between the two towers took place from the figures. This phenomenon could also be seen by both El-centro wave and Taft wave test, see fig.11. The lateral acceleration at the 37rd floor was larger than the 54th floor $(A_{max}=0.225g^* C_a)$.

X-Acceleration(g)   Y-Acceleration(g)   X-Displacement(mm)   Y-Displacement(mm)

fig.9 Max.acceleration distribution   fig.10 Max. displacement distribution

table 2 Comparison on frequency results (Hz) (elastic stage)

Mode	Fe1x	Fe1y	Fe2x	Fe2y	Fe3x
Tested	4.88	5.07	15.80	15.20	20.66
Calculated*	3.71	4.00	11.12	10.06	16.81

*note: calculation results converted from the prototype into the model.

Table 3 Frequency results(Hz) (elastoplastic stage)

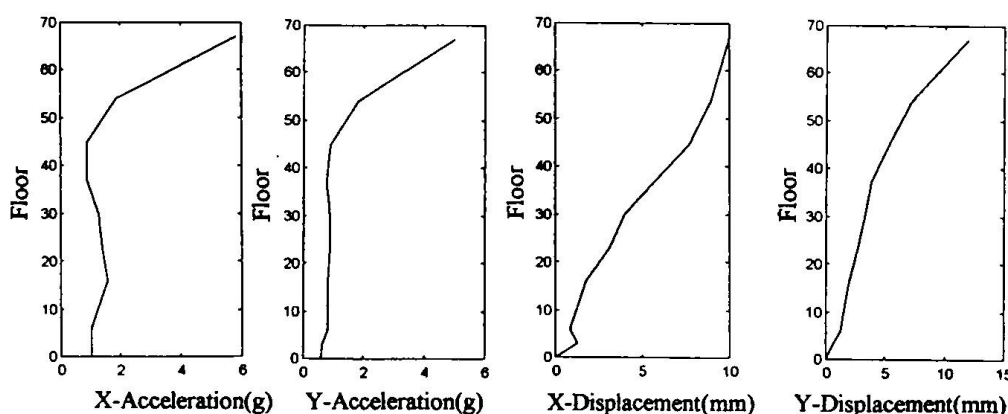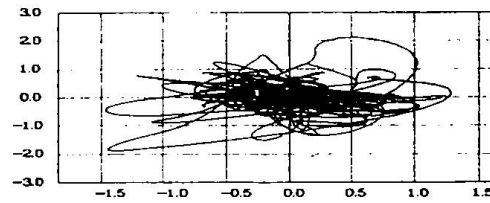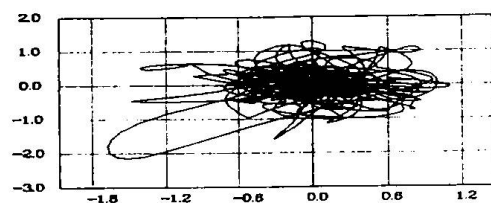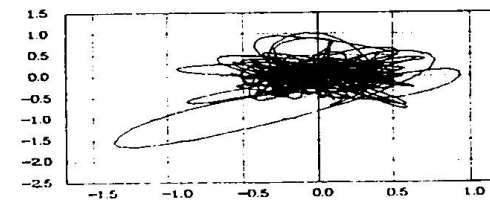| Mode	Fp1x	Fp1y	Fp2x	Fp2y	Fp3x
Tested	3.76	4.32	14.09	12.02	18.03
Fpi/Fei	77%	85%	89%	79%	87%
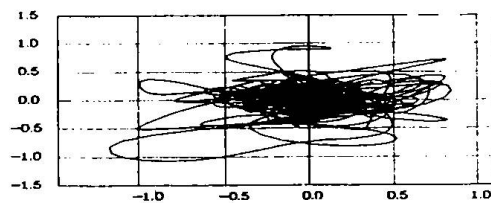
(a) At the 6th floor   (c) At the 45th floor

(b) At the 37rd floor   (d) At the 54th floor

fig.11 acceleration track at different elevations $(A_{max}=0.225g^*C_a)$

Conclusion

1. Tested structural frequencies, vibration mode shapes and other dynamic response characters of the S.R.C. model were presented in this paper.

2. Structural frequencies declined obviously when the model experenced different intensity of earthquakes.

3. The two towers connected by the overbridge had considerable relative movement, the lateral displacement and acceleration at middle part were enlarged during vibration.

4. The calculated frequencies approached to the test result. The differences came mainly from the rigid floor assumption and the concrete module without considering steel ratio.

5. MDF shear model is not suitable for the analysis of the complex building. Shape steel ratio should be considered in the stiffness calculation of S.R.C. members.

6. The S.R.C. column details have reliable working behavior. However, very severe cracks appeared on the bottom of the neck when the input acceleration reached to 0.225g. So the connection part should be more safely designed.

Keywords

S.R.C Structure, Dynamic Test, Modeling Techniques, Earthquake Resistant Design

References

[1]. Design Code for Earthquake Resistant Building, GBJ11-89, April,1990, China.
[2]. Structural Design and Construction Standard for High-rise Buildings in Reinforced Concrete, JGJ 3-91, 1991, China.
[3]. G.M.Sabnis,H.G.Harris,R.N.White,M.S.Mirza,Structural Modeling and Experimental Techniques, Prentice-Hall, 1983.

Seismic Design of Composite Semi-Continuous Frames

Roberto T. LEON
Professor
Georgia Inst. of Technology
Atlanta, GA, USA

Roberto Leon received his
PhD from the U. of Texas
at Austin in 1983, and taught
at the U. of Minnesota for 10
years. He joined Georgia Tech
in 1995.

Summary

The poor performance of fully restrained frames during the Northridge and Kobe earthquakes has led to a reassessment of the required ductility in steel frames subjected to seismic loads. From the ductility standpoint, one possible alternative to FR frames is the use of semi-continuous or partially restrained (PR) frames. PR connections can undergo large cyclic rotations, exhibit excellent hysteretic behavior, and result in highly redundant, tough structures. However, PR connections are generally not full strength (FS), and their satisfactory performance depends on understanding their cyclic behavior and careful detailing during the design process.

1. Introduction

Although American steel design codes have recognized the use of partially restrained (PR or semi-continuous) construction since 1946, the codes do not provide any specific guidance for their design. However, there has always been extensive use made of these connections in low-rise construction in areas where wind force govern the lateral load design of the structure. For this situation the code has allowed a two-step analysis, where the connections are assumed as pinned for gravity loads and rigid for gravity loads. Extensive parametric studies have shown that under a allowable stress design (ASD) format, this approach provides a safe and economical design [Ackroyd 1987]. In the past few years there has been a trend towards ultimate strength design spurred by the increasing recognition both that seismic design criteria need to be implemented in large areas of the US and that this format has been adopted in codes worldwide. Although under the Load and Resistance Factor Design (LRFD or ultimate strength design) approach the two-step approach has been maintained, there is increasing recognition that more advanced design techniques need to be implemented for the design of structures with PR connections.

The 1994 Northridge earthquake, which severely damaged modern fully rigid (FR) steel moment frames, indicated that there is a need to provide redundancy and toughness to steel frames. Inspections after this earthquake showed that numerous buildings, in which a large number of rigid connections fractured, performed well because of the resistance of the gravity connections. The latter are PR, partial strength connections whose interaction with the slab provided adequate strength and stiffness to resist the lower base shear demand resulting from the increased flexibility of the structural system. While the composite interaction observed during the Northridge earthquake was unintentional, the concept of a partially-restrained composite connection (PR-CC)

has been around for many years. Recently, Leon et al. [Leon 1990] among others have shown that these connections possess enough strength, stiffness, and ductility to resist wind and moderate seismic loads. The concept of PR-CCs is currently being applied in the Eastern US to low-rise, commercial structures with large footprints where numerous column lines allow the cumulative effect of the connections to provide the required lateral resistance. Recently two design documents have been developed [Leon et al. 1996; ASCE Design Guide to appear in print in early 1998] to give detailed, step-by-step design procedures. More importantly, the new drafts of both the AISC Seismic Specification [AISC 1997] and the model code promulgated by the National Earthquake Hazard Research Program (NEHRP) [NEHRP 1997] explicitly include this system and assign it specific force reduction, displacement amplification, and system redundancy factors. In this short paper the key aspects of PR-CC design will be discussed and its implementation in codes explained.

2. Partially Restrained Composite Connections and Frames

Partially restrained, or semi-rigid, composite connections (PR-CC) are modified steel frame connections in which additional strength and stiffness are provided by the floor slab. These connections require the addition of shear studs and slab reinforcement in the negative moment regions adjacent to the columns, and utilize the slab reinforcement as the top element of the connection (Fig. 1).
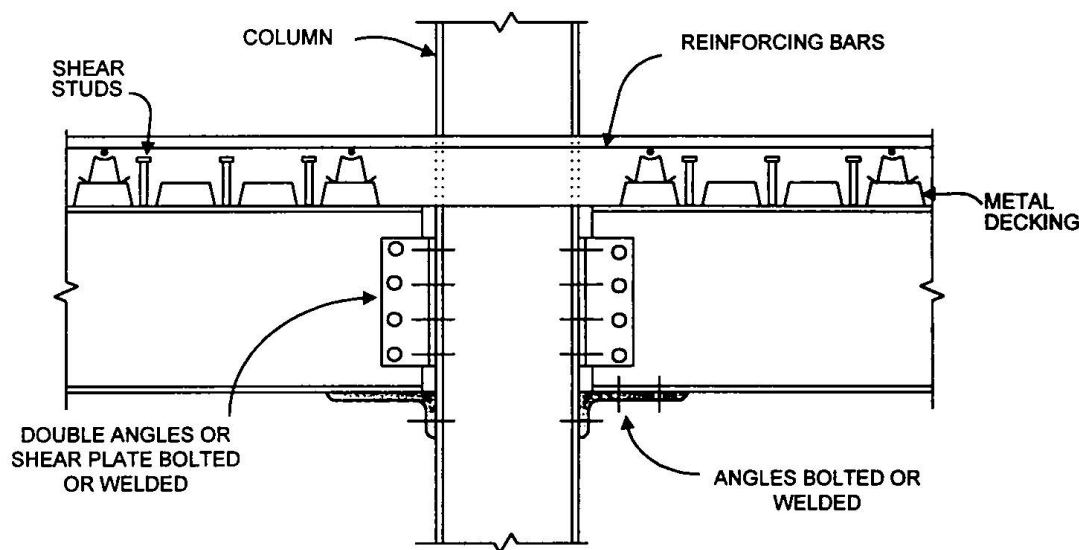
Figure 1 - Typical partially-restrained composite connection (PR-CC).

Several important characteristics of PR-CC design, with particular emphasis on their effect on design procedures and the dynamic performance of the frame, need to be understood:

1. PR-CC connections are typically partially restrained insofar as stiffness and partial strength insofar as ultimate capacity. The designer is free to choose an optimal combination of strength and stiffness for the particular application. Parametric studies indicate that the most efficient connections are those that provide around 70% to 80% of the bare steel beam plastic resistance and have a service stiffness of 10 to 15 time that of the beam [Leon and Forcier 1992].

2. Connection flexibility has a significant impact on the serviceability limit state, and trial designs indicate that the required connection stiffness for drift control under wind loads is the governing parameter in the design. Because of the non-linear characteristics of the moment-rotation curves for PR-CCs, conventional analysis and design procedures, based on rigid, full-strength connections cannot be utilized directly to obtain the forces and deformations in these structures. For the service load level, the use of linear springs in the analysis can be justified if a conservative secant stiffness, rather than the initial tangent stiffness, is used.

3. As the ultimate strength of the connections is reached, plastic hinges will form at the ends of beams. Under increasing monotonic lateral loads, a stable frame-sway mechanism will result only if the connections provide large ductility and a dependable hardening regime. In addition, under cyclic load reversals, the losses of strength and stiffness with cycling have to be controlled so the system provides adequate energy dissipation capacity. For gravity loads, it is recommended that the rotational capacity be at least 0.05 radian. For lateral loads the cyclic rotational capacity must exceed 0.03 radian with less than 20% loss of strength. These stringent requirements mean that careful attention must be paid to the connection detailing.

4. Composite action will resist only loads applied after the concrete has hardened (live, wind, and earthquake loads). Thus the beams need to be checked for construction and dead loads as either simply supported beams or beams with weak PR connections.

5. The effect of the flexibility of the connections on the dynamic performance of the structure is to lengthen its period, and thus reduce its base shear demand. The change in period is very susceptible to the assumption of initial stiffness for the connection. The use of a complete non-linear moment-rotation curve, with the period computed based on the initial stiffness, will result in very small changes in period vs. that of a FR frame. On the other hand, periods computed based on a secant or tangent stiffness near initial yield, can produce large period shifts. It is not clear yet which definition of stiffness should be used for code-type calculations.

6. Analytical studies have shown that structures with PR connections do not necessarily drift more than similar structures with FR connections. In general, the drift of frames with PR connections is within ±20% of that of similar FR frames. The results are sensitive to ground motion amplitude, frequency content,

7. duration, and distribution of energy input with time.

8. The problem of dynamic stability of a frame with PR connections is fundamentally different from that of a frame under monotonically increasing loads. Because the loads are inertial and random, the temporary formation of a mechanism does not imply the collapse of the structure. The study of plastic hinge distribution in PR frames subjected to ground motions indicate that local mechanisms disappear within a few time steps (a typical step is 0.02 sec. or smaller).

9. It is unlikely that the number of frames required to resist lateral loads in a PR frame will remain the same as in a similar FR one. More frames, and in fact all frames if possible, should be used to resist lateral loads in a frame with PR-CCs. This results in a highly redundant and tough structural system.

10. PR-CC connections use continuity and strength that is already built in into many existing structures. Some empirical code provisions and long-established criteria already take the effects of floor slabs and partial restraint into account indirectly. Examples of this include code provisions for calculation of natural periods and the traditional limits for service deflections and drift. Thus, designers need to exercise care when assessing the impact of PR-CC in their designs.

3. Code Implementation

It is important to understand that although many design methods have been proposed for PR frames, there is not yet a consensus in the profession on how to analyze and design PR, partial strength structures. The most important differences between analyses of PR frames and traditional FR steel frames are the need to include both the non-linear behavior and partial strength characteristics of the connections into the analysis of the former. Proposed code language enabling the use of PR-CC construction [AISC 1997, NEHRP 1997] does not contain any specific suggestions for the analysis of PR frames. The references cited by these codes suggest that for preliminary design of regular frames for gravity and wind loads, a two-step approach (service level and ultimate strength) is reasonable. Regular frames are defined as those meeting strict requirements insofar as distribution of strength and stiffness in both plan and elevation. In addition, both codes limit the use of the system to structures under 40 m in height, and to structures not housing critical facilities. The force reduction and displacement amplification factors used for design are equivalent to those permitted for intermediate steel frames. The latter are a class of structures where only minimum seismic detailing is required. Both codes [AISC 1997, NEHRP 1997] set the force reduction factor at 6.0, the displacement amplification factor (inelastic/elastic displacement) at 5.5, and its horizontal overstrength factor is 2.75. Because these new codes have significantly larger design base shears built-in, it is not possible to directly compare them with those given in other seismic codes.

For the service level, an elastic analysis with linear springs can give reasonable values for the required connection stiffness. However, as noted earlier, because the connections have non-linear moment-rotation characteristics, it is necessary for preliminary design to utilize a conservative secant stiffness rather than the initial tangent stiffness for the connections. For the ultimate strength limit state, a simplified second-order plastic analysis [Horne and Morris 1982], based on empirical factors derived from extensive parametric studies [Leon et al. 1996], can provide a conservative estimate of the collapse strength of the frames if the regularity and detailing criteria are met.   For final design, a complete non-linear analysis under both proportional and non-proportional loading is suggested.   For the case of seismic forces, both proposed codes [AISC 1997, NEHRP 1997] require that non-linear, time-history analyses be run to determine the overall performance of the system.

Because PR-CCs incorporate the floor slab into the frame action, it is important to model this behavior in the analysis and design of PR-CC frames. For analyses using an equivalent static load, it is suggested that an equivalent prismatic moment of inertia (I_{eq}) be used for the beam members. This moment of inertia can be taken as [Leon et al., 1996]:

$$I_{eq} = 0.6 I_{LB+} + 0.4 I_{LB-}$$
(1)

where I_{LB+} and I_{LB-} are the lower bound moments of inertia in positive and negative bending respectively.

Preliminary column stability checks should be carried out by assuming that the effective length factor includes the effect of the spring (ASCE 1997). This can be accomplished by assuming a modified I_{eff} for the girder as given by Eq. (2).

$$I_{eff} = I_{eq} \left(\frac{1}{1+3\alpha}\right) \quad \text{where} \quad \alpha = \frac{2 E I_{eq}}{L_g k_{conn}}$$
(2)

Because for an unbraced frame under lateral loads one connection will be loading and one unloading, the values of the connection stiffness (k_{conn}) on either side of the connection vary. For initial calculations, k_{conn} should be taken as equal to the secant stiffness at the service load level for the unloading side, and as the hardening stiffness of the connection for the loading side.

The force transfer mechanism for this type of connection is shown in Fig. 2. The tensile forces produced on the left side of the connection (sagging or negative moment) are transferred by bearing on the column flange on the other side of the connection through a strut-and-tie mechanism.
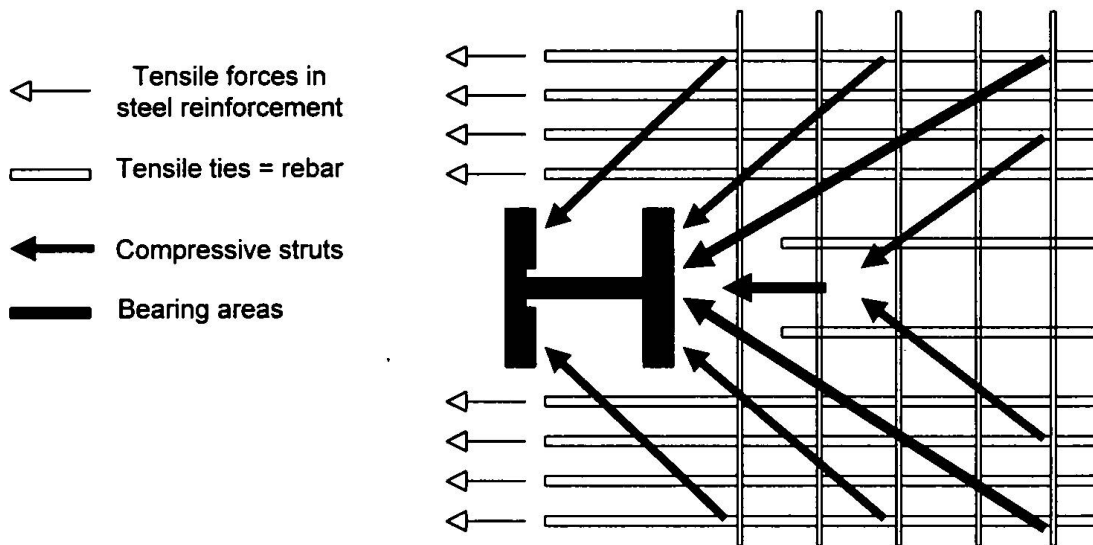

Figure 2 - Force transfer mechanism (simplified strut-and-tie model).

The design of the connections is predicated on achieving a ductile, reliable limit state (yielding of the slab steel under negative moments, for example) well before any brittle failure mechanism (buckling of the bottom beam flange or shearing of the bolts in the seat angle, for example) can occur. The design procedure requires that the following limit states be checked:

1. Shear strength for bolts attaching the seat angle to the beam.

2. Bearing strength at the bolt holes.

3. Tension yield and rupture of the seat angle.

4. Tension strength, including prying action, for the bolts connecting the beam to the column.

5. Shear capacity of the web angles.

6. Block shear capacity of the web angles.

7. Number and distribution of slab bars, including transverse reinforcement, to insure a proper strut-and-tie action at ultimate.

8. Concrete bearing stresses

9. Number and distribution of shear studs to provide adequate composite action.

10. Column panel zone (check the need for column stiffeners).

Design tables for PR-CC connections that meet all of these criteria are available (Leon et al. 1996).

The following detailing rules for the slab steel for structures subjected to seismic forces intend to insure a smooth transfer of forces into the columns, and delay strength degradation with cycling:

1. The slab reinforcement should consist of at least six longitudinal bars, not welded wire fabric, placed symmetrically within a total effective width of seven column flange widths.

2. Transverse reinforcement, consistent with a strut-and-tie model, shall be provided. In the limit this amount will be equal to that of the longitudinal reinforcement.

3. The maximum bar size allowed is 19 mm and the transverse reinforcement should be placed below the top of the studs whenever possible.

4. The slab steel should extend for a distance given by the longest of $L_x/4$ or 24 bar diameters past the assumed inflection point. At least two bars should be carried continuously across the span.

5. All splices shall be designed in accordance with seismic requirements for concrete structures.

6. Whenever possible the space between the column flanges shall be filled with concrete. This aids in transferring the forces and reduces stability problems in the column flanges and web.

4. Conclusions

While the recognition by design codes of the potential of PR-CC connections is encouraging, several important practical issues still need to be clarified. The first is the need for advanced analysis techniques, which is necessary at this stage because little is known about the system behavior for this type of frame. The second is the development of simplified procedures to take into account the strengthening and stiffening effect of the slab on the whole system and not just the connections. A third important practical issue is the development of simplified formulae for the calculation of the natural period of these structures. Finally, it is necessary to investigate the effect of higher modes on the dynamic performance of these frames since non-linear dynamic analysis indicate that this phenomenon may be of greater importance for PR than for FR frames.

5. References

1. Ackroyd, M.H., 1987. "Simplified Frame Design of Type PR Construction," AISC Engineering Journal, Vol. 24, No. 4, pp. 141-146.

2. AISC, 1997. Seismic Provisions for Structural Steel Buildings, American Institute of Steel Construction, Chicago, IL.

3. ASCE Task Group on Effective Length, 1997. "Effective Length and Notional Load Approaches for Assessing Frame Stability," ASCE LRFD Committee, ASCE, New York.

4. Horne, M.R., and Morris, L.J., 1982. Plastic Design of Low-Rise Frames, The MIT Press, Cambridge, MA.

5. Leon, R. T., 1990, "Semi-Rigid Composite Construction," Journal of Constructional Steel Research, Vol. 15, Nos. 1&2, pp. 99-120.

6. Leon, R. T., and Forcier, G.P., 1992, "Parametric Study of Composite Frames," in Connections in Steel Structures II, (R. Bjorhovde et al. eds.), AISC, Chicago , pp. 152-159.

7 . Leon, R.T, Hoffman, J.J., and Staeger, T., 1996. Partially Restrained Composite Connections, Steel Design Guide 8, AISC, Chicago, 57 pp.